THESIS

TRANSIENT MODELING OF AN AMBIENT TEMPERATURE SOURCE CENTRIFUGAL COMPRESSOR STEAM GENERATING HEAT PUMP.

Submitted by

Kelly Patrick Ryan

Department of Mechanical Engineering

In partial fulfillment of the requirements

For the Degree of Master of Science

Colorado State University

Fort Collins, Colorado

Fall 2024

Master's Committee:

Advisor: Todd M. Bandhauer

Brett C. Windom
Daniel R. Herber

ABSTRACT

TRANSIENT MODELING OF AN AMBIENT TEMPERATURE SOURCE CENTRIFUGAL COMPRESSOR STEAM GENERATING HEAT PUMP.

As the US electricity grid transitions to renewable power generation, electrifying end-uses that are currently fossil fuel fired presents a promising path towards deeper decarbonization, and next generation high temperature heat pumps are a viable solution for decarbonizing fossil fuel fired steam boilers. These next-gen systems require a higher degree of design complexity and more finely tuned control strategies than existing systems, and therefore can benefit from complex transient modeling that has not been previously implemented for these types of systems. A transient study of a novel steam-generating heat pump with steam delivery temperature of 150°C was conducted using physics-based simulation software. The model used manufacturer supplied performance data to calibrate each competent, providing reliable preliminary validation to the model. The model was set up to match the configuration of a prototype system constructed at Colorado State University. It was found that the results of the transient model agreed well with the steady state model of the heat pump at the design point. Transient conditions including cold startup to full load operation, full load operation to part load operation, and part load operation back to full load operation were modeled and the system was found to operate with stability. Compressor and expansion valve performance was investigated. Compressors were found to operate within their performance maps for both steady and transient operation. A control strategy was developed for the expansion valves to prevent liquid ingestion when transitioning to turndown operation. The system COP was predicted for both full and part load operation and in transition between them.

ACKNOWLEDGEMENTS

There are so many amazing people in my life that have led me to where I am today. First and foremost, I would like to thank Dr. Todd Bandhauer for everything he has provided me with during the past 2+ years. I was fortunate enough that during my junior year as an undergraduate I met a friend who already worked in Dr. Bandhauer's lab and informed me of the interesting projects taking place at the REACH CoLab. His passion and pride in his lab and research led me to join his team, the REACH CoLab, for my Senior Research project and ultimately continuing into graduate school. Dr. Bandhauer has always treated myself and others as equals and it has been a pleasure to work beside him on my graduate research. I can't wait to see what the future holds as I continue working at AtmosZero for the coming years!

Of course, the completion of this work would not have been possible without the support and contribution of others in the REACH CoLab. I cannot thank Joe Huyett, Maddy Siegel, Wale Odukomaiya, Nick Roberts, and Meha Setiya enough as they have been incredibly important in my development as an engineer and contributor in the lab. Since day 1 they have provided a tremendous amount of time and support. There is simply no way that I would have been able complete this thesis without them. I'd also like to thank Taylor Stoll for helping to read, review and further my work.

Lastly, I would like to thank my friends and family for all of their love and support. Their constant reassurance and belief in my future success has been an indispensable tool throughout my academic experience.

TABLE OF CONTENTS

LIST OF TABLES

LIST OF FIGURES

NOMENCLATURE

Nomenclature		***Subscripts***	
COP	Coefficient of performance	abs	Absolute Temperature
GWP	Global warming potential	avg	Average
PID	Proportional-Integral-Derivative	comp	Compressor
SC	Subcooled region	elec	Electrical
SH	Superheated region	evap	Cooling cycle evaporator
SLHX	Suction line heat exchanger	in	Inlet
TP	Two-phase region	out	Outlet
TD	Turndown	r	Refrigerant
VFD	Variable frequency drive	min	Minimum
LP	Low pressure	max	Maximum
HP	High pressure	s	Isentropic property
LIMS	Liquid Ingestion Mitigation Strategy	th	Thermal
UA	Heat exchanger overall heat transfer coefficient-area	ref	Reference property value
Variables		op	Operational property value
Cp	Specific heat capacity [kJ kg^{-1} K^{-1}]	corr	Corrected mass flow
h	Enthalpy [kJ kg^{-1}]		
$\dot{m}$	Mass flowrate [kg s^{-1}]		
P	Pressure [kPa]		
ΔP	Pressure loss [kPa]		
$\dot{Q}$	Rate of heat transfer [kW]		
$\dot{W}$	Rate of work transfer [kW]		
ε	Heat exchanger effectiveness [-]		
T	Temperature [°C]		
η	Efficiency [-]		

CHAPTER 1: Introduction

1.1 Motivation

Since the turn of the 21st century, the effects of human caused atmospheric carbon emissions on the global climate have become more and more apparent, as evidenced by the 2018 United Nations International Panel on Climate Change Special Report that details the impacts expected if global warming were to exceed 1.5C above pre-industrial levels [1]. As a result, there have been increasing efforts to develop and deploy technologies that provide carbon-free energy ensuring the same quality of life and economic benefits that fossil fuels afforded humankind over the last 150 years.

As show in Figure 1-1 (A), industrial process heat was responsible for about one fifth of global CO2 emissions in 2016 [2]. In the US, industrial heat demand in the range of 100-200°C makes up about 25% of the total industrial process heat demand as shown in Figure 1-1 (B), most of which is steam-supplied [2], [3]. Most electricity in the US is still generated using fossil fuels, but the share of electricity generated from renewables has been increasing in recent years [4]. As the grid becomes decarbonized, electrifying end-uses that are currently fossil-fuel-fired offers a promising path towards deeper decarbonization. Because of the large cost and time commitment associated with electrification, beginning this transition long before the grid is fully decarbonized can help avoid a lag in emissions reduction progress.

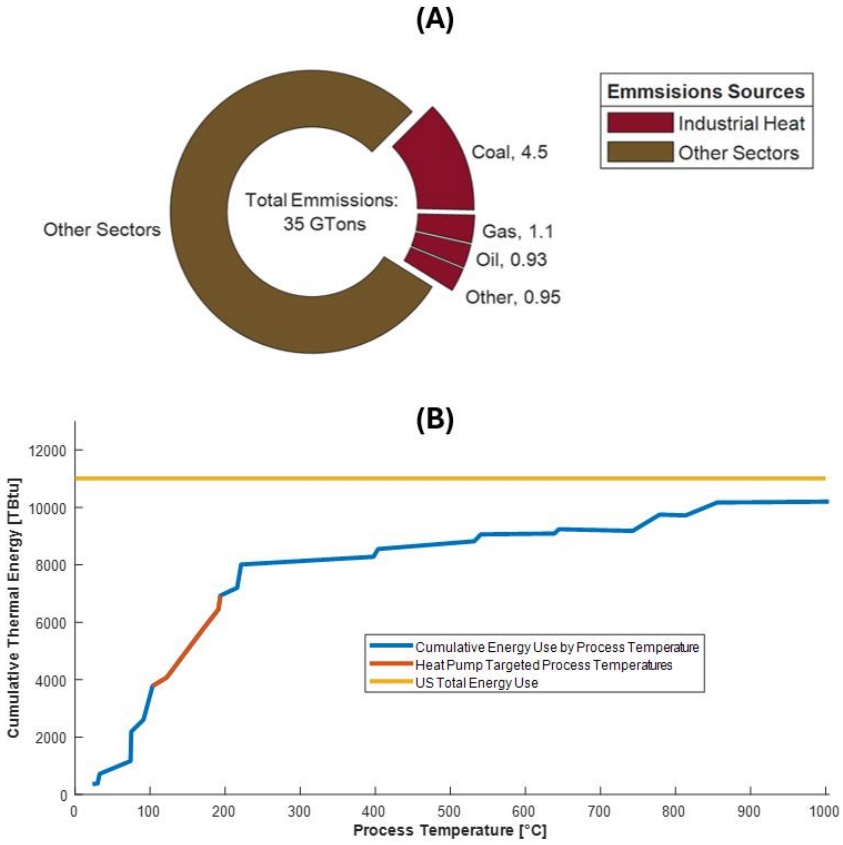

Figure 1-1: Emission reduction potential provided by the deployment of electrified heat pumps, **(A)** – Emission sources from Industrial heat production from [2], **(B)** – Total thermal energy use by process temperature from [5] and range of targeted process temperature typical of steam generating heat pumps.

Renewably powered, electrified heat pumps stand to disrupt traditional means of supplying industrial heat and provide significant reductions in carbon emissions [3]. Heat pumps are particularly advantageous because they supply more than one kilowatt of heat for every kilowatt of electricity they consume, with this ratio being known as the Coefficient of Performance or COP and being dependent on the operational temperatures of the heat pump. The temperature range targeted for heat pump deployment is 100-200°C. This range was selected because 100°C is the minimum temperature steam can be generated at atmospheric pressure. 200°C was selected for the upper limit because of several factors including refrigerant decomposition temperature, decreasing

COP with increasing delivery temperature or the need for a waste heat supply stream, material temperature constraints in compressor construction, and increasing system cost with delivery temperature.

1.2 Methods for Improvement

As stated above, most low to medium temperature process heat is steam supplied, the generation of which has historically been accomplished through combustive heating. Recently interest in electrified heat generation has increased following the need for decarbonization [2]. Electrical resistive heating and heat pumping are the two technologies available to electrify industrial heat. Combustive heating and electrical resistive heating must always, according to the 2nd law of thermodynamics, have an efficiency less than one, whereas a heat pump is a machine that supplies more heat energy to its high temperature reservoir than it consumes at the compressor(s) [6]. Because heat pumps have COPs which can be greater than one as shown in Equations 1 and 2 , they can produce steam at a reduced operating cost compared to resistive boilers for a given application, making them an attractive option. The maximum theoretical COP, also known as the Carnot COP, given in Equation 1 is governed by the temperature difference of the heat source and heat sink.

$$COP_{max} = \frac{T_{abs,hot}}{T_{abs,hot} - T_{abs,cold}} \quad (1)$$

$$COP = \frac{\dot{Q}_{steam}}{\dot{W}_{electric}} \quad (2)$$

1.3 Ambient Heat Availability

A limiting factor for most existing 100°C+ industrial heat pump technologies is the requirement of a waste heat stream as the low temperature source [7], [8]. Due to the significant heterogeneity of waste heat sources across industrial settings [5], waste-heat integrated heat pumps are deployable only in certain contexts and must be custom designed based on site-specific requirements. Using ambient heat as the low temperature source eliminates the need for a waste heat stream by absorbing the required heat directly out of the atmosphere. This enables deployment across many potential applications, without requiring bespoke engineering, greatly reducing capital and implementation costs.

There are two main limitations for ambient sourced heat pumps. The first limitation is the fact that the Maximum COP decreases with increasing source sink temperature. This is significant due to the large range of seasonal and daily variation in ambient temperature. The second limitation is fluctuating ambient temperature requiring a dynamic controls response. Not only does the heat pump need to be able to operate steadily at any given ambient temperature, it needs to be able to adjust its operation in real time as the temperature changes.

1.4 Complex System Interaction Requires Transient Modeling

Due to several factors including the varying and somewhat unpredictable nature of hourly to daily temperature variation, and varying demand from industrial steam users, an ambient-source heat pump must be able to perform well over a range of operating conditions. While the outdoor

temperature can be predicted with relative accuracy for the near future, industrial processes do not have the luxury of scheduling plant operations based on daily or weekly weather predictions. As such the heat pump must be able to deliver the requested steam load regardless of the outdoor temperature. To achieve the best operation possible, transient models of the system can be utilized to optimize compressor and expansion valve (EXV) operation based on steam demand and outdoor temperature, as well as aid in optimizing component performance and configuration by allowing for much more rapid testing and evaluation than a physical prototype test.

1.5 Boiler 2.0

In this work a novel steam generating heat pump system proposed by AtmosZero named Boiler 2.0 is investigated. AtmosZero is developing and rapidly commercializing a novel, centrifugal compressor driven, cascade, air-sourced, steam generating heat pump to address the need for decarbonized steam generation. A system overview pictured in Figure 1-2.

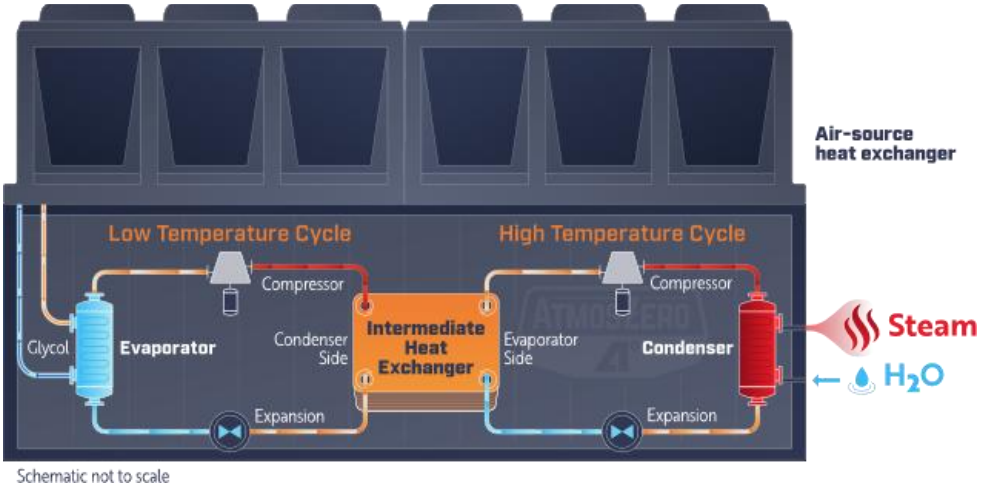

Figure 1-2: AtmosZero high level heat pump overview

CHAPTER 2: Literature Review

2.1 Overview of Heat Pump Technology

Compression heat pumps are engineered systems that use mechanical work to move thermal energy from a reservoir of low temperature to a reservoir of high temperature [6]. In general, this can be accomplished using heat-engine thermodynamic cycles which are operated in reverse, such that they consume mechanical work rather than producing it [6]. Thermally driven, also known as sorption heat pumps will not be considered here due to the fundamental differences from compression heat pumps in their operation and construction. Thermally driven heat pumps take advantage of chemical processes rather than purely physical ones, and as their name suggests are powered by thermal energy rather than electrical energy, so they don't offer the same electrified decarbonization pathway as compression heat pumps.

In practice, there are two thermodynamic cycles used for this purpose: The reversed Rankine cycle, and the reversed Brayton cycle [6]. The reversed Rankine cycle, more commonly known as the vapor compression cycle, uses evaporation and condensation at different saturation pressures to move heat [6]. Due to the use of the latent heat of vaporization by vapor compression systems, heat can be moved more efficiently. The Breyton cycle uses only sensible heat, compressing and expanding a gaseous working fluid.

There are three main attributes that can be used to group compression-type heat pumps into meaningful categories. The first is the type of thermodynamic cycle used by the system, the second is the type of compressor that is used in the system, and the last attribute is the use of a single stage configuration or a cascade configuration with multiple cycles in series.

Vapor compression heat pumps, like all heat pumps, move thermal energy from a low temperature source to a high temperature sink. vapor compression heat pumps do this by boiling a

refrigerant at the low temperature source, compressing the vapor and then condensing it at the high temperature sink before flashing the liquid back to the original pressure. Boiling and condensation of pure substances and azeotropic mixtures occur at constant temperature and pressure which is advantageous to heat pump system because it can reduce the total temperature lift of the refrigerant for a given set of reservoir temperatures thereby increasing the Carnot COP. The temperature lift is reduced by this isothermal heat transfer condition because a smaller average temperature difference is required between the refrigerant and the sink/source to drive heat transfer than would be required in a non-phase-change medium using only sensible heat. As a result, the bulk refrigerant temperature is higher at the source and lower at the sink which translates to a lower total temperature lift. The vapor compression cycle is visualized using the Pressure vs. Enthalpy (P-h) and Temperature vs. Entropy (T-s) diagrams pictured in Figure 2-1 and 2-2. In each of these diagrams the refrigerant begins at state 1 as a saturated or slightly superheated vapor. It is then compressed to a higher pressure and temperature at state 2. The deviation from a vertical line between state 1 and state 2 in the T-s diagram (Figure 2-2) is due to the isentropic efficiency of the compressor, with a vertical line representing an isentropic efficiency of 100%. The hot vapor is then condensed from state 2 to state 3. From state 3 to state 4 the vapor is expanded back to its original pressure. From state 4 to state 1 the two-phase mixture resulting from the expansion is boiled, returning the refrigerant to its original vapor state. The Top and bottom Cycles use R1233zd(E) (a pure substance) and the R513a (an azeotropic mixture) respectively.

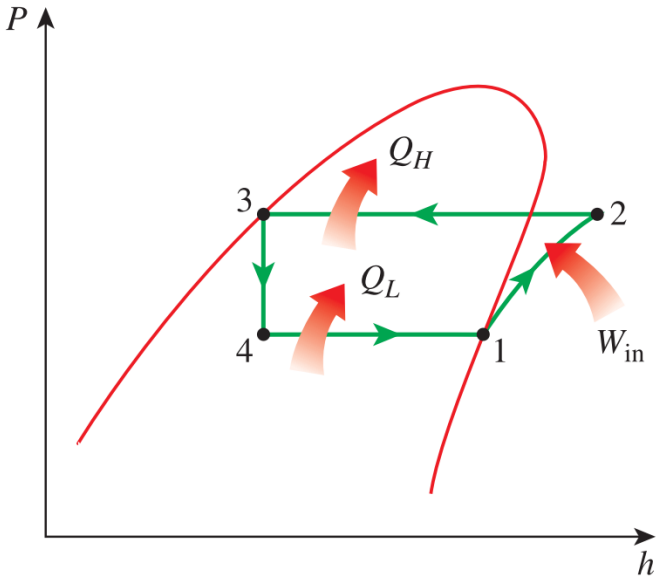

Figure 2-1: Example of a vapor compression cycle represented on the P-h diagram, from [6]

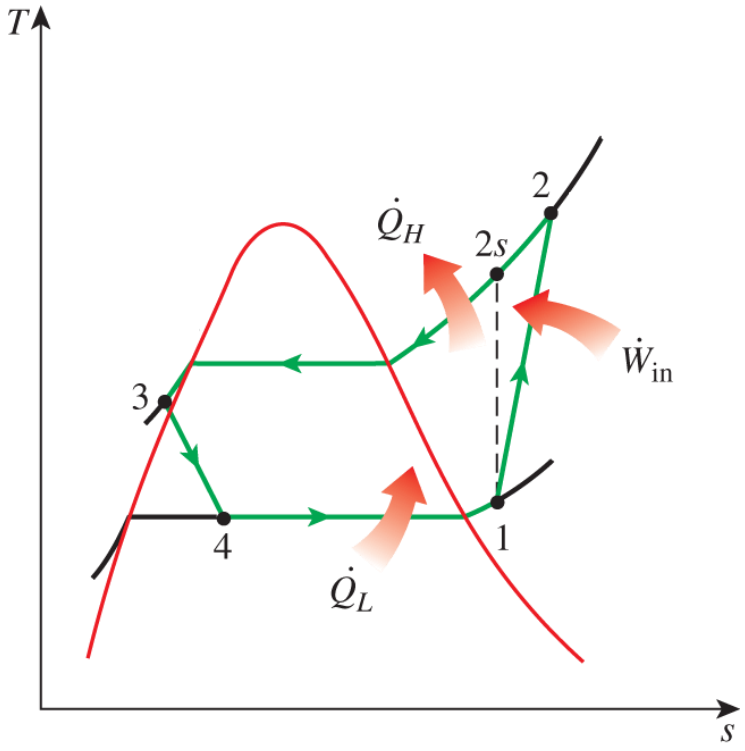

Figure 2-2: Example of a vapor compression cycle represented on the T-s diagram, from [6]

A cascade heat pump uses two independent cycles to achieve a higher COP for a given temperature lift by reducing the required compressor work to achieve the same temperature lift as well as increasing the latent heat capacity of the refrigerant stream for a given mass flow rate, as shown in Figure 2-3. Cascade cycles can also use multiple refrigerants allowing each cycle to operate at a more advantageous place on the vapor dome than can be achieved with the same refrigerant being used in both cycles.

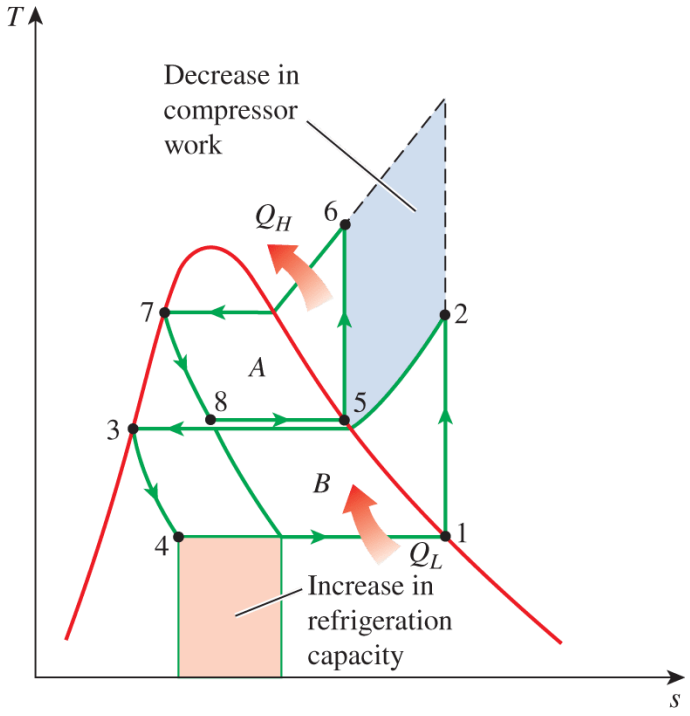

Figure 2-3: Effects of utilizing cascade cycle as compared to a single cycle, from [6]

A variation of the vapor compression cycle is the Transcritical Vapor Compression cycle. This cycle evaporates the working fluid at low temperature and pressure then compresses the fluid above its critical point, transitioning it into a supercritical fluid. Heat is rejected from the supercritical fluid in a gas cooler before it is expanded back to a two-phase subcritical state and the process begins again. Supercritical systems are advantageous over traditional vapor

compression systems because they don't require specialized refrigerants to achieve high delivery temperatures above that of commonly used and commercially available refrigerants but can still take advantage of the phase change in the evaporator. Transcritical cycles cannot, however, take advantage of isothermal heat transfer in the condenser because the supercritical fluid does not condense like a vapor, reducing the maximum COP of the system for a given set of source and sink temperatures. Additionally, gasses with higher molecular weights are easier to compress efficiently because they require lower compressor wheel tip speeds and/or less compression stages due to the greater momentum possessed by the individual molecules compared to that of lighter media traveling at a given speed [9]. Supercritical CO_2 systems also require much higher pressures due to the critical pressure of CO_2 being around 7400 kPa as opposed to the highest system pressure seen in the current work of ~3000 kPa [6]. The combination of these factors makes supercritical CO_2 less advantageous than traditional vapor compression for the current application.

2.2 Considerations in Compressor Selection

The maximum COP shown in Equation 1 decreases with increasing temperature lift, so employing the most efficient compressor type available will therefore improve the viability of high lift heat pumps [6]. As such, optimizing compressor operation is especially crucial to the success of high lift heat pumps. There are many types of vapor compressors available, but they all fall into one of two categories: positive displacement of centrifugal. Positive displacement compressors work by reducing the volume of an enclosed space and they are available in a variety of configurations including piston, screw, sliding vane, rotary and others. Centrifugal compressors use a moving blade row to do work on a continuously moving fluid thereby dynamically changing the stagnation pressure of the fluid [9]. The use of centrifugal compression allows for the potential of higher design point efficiency but inherently requires more sensitive control than positive

displacement machines due to the dynamic nature of the centrifugal compression process [10], [11], [12], [13], [14]. Centrifugal machines also offer additional advantages over positive displacement machines including lower maintenance cost, lower design complexity, high reliability, quiet operation, and no requirement of oil-refrigerant contact for lubrication [9], [14]. This is accomplished through the use of specific bearings including but not limited to sealed bearings, refrigerant lubricated bearings or magnetic bearings. The elimination of the need for lubricating oil in direct contact with the refrigerant not only reduces the compressors maintenance needs (no need for oil changes) but also reduces the potential for fouling to occur in any of the various heat exchangers, further increasing overall system reliability and performance.

High temperature heat pumps that operate on waste heat have traditionally used positive displacement compression. These systems inherently have a lower temperature lift than ambient sourced heat pumps, and therefore their maximum COPs are much higher. This results in the overall system performance being less sensitive to compressor efficiency. The benefit gained from increased rangeability for the compressor outweighs the benefit from increased design point efficiency in these waste heat driven systems.

Design criteria for centrifugal machines can be derived from the generalized Cordier diagram shown in Figure 2-4. The Cordier analysis method for machine design and selection uses nondimensionalized quantities of rotor rotational speed (specific speed, Ns) and machine throat diameter (specific diameter, Ds) to predict the most efficient machine type size and speed for a given set of operating conditions [9], [12]. For centrifugal compressors, the highest efficiency machines are found in the region of approximately $60<Ns<300$ and $0.6<Ds<3$ [12]

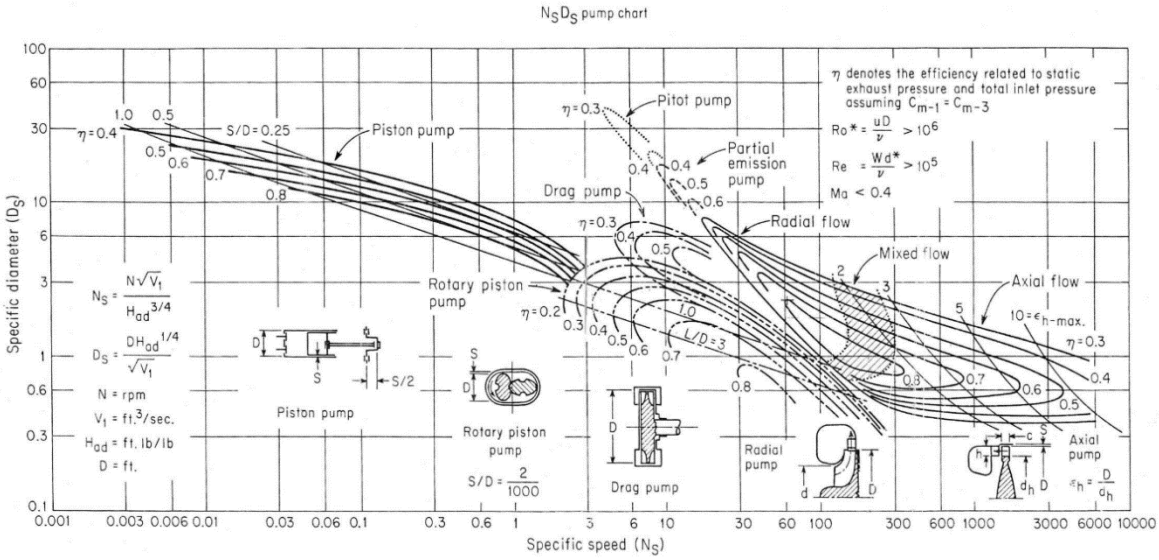

Figure 2-4: General Cordier Diagram for pumping machinery [12].

2.3 Chillers

Chillers and heat pumps are the same type of machine being used for different purposes, and as such studies concerning centrifugal chillers are particularly applicable to this work. Chillers do, however, have inherently lower temperature lifts because the desired temperature of chilled water is much closer to ambient than that of steam. Chillers are available in both positive displacement and centrifugal configurations. The selection of compressor type is made for the specific application of a given chiller based on the tradeoff between centrifugal having higher design point efficiency and capacity, and positive displacement having wider rangeability. Centrifugal chillers are the most efficient type of chiller at the design point but suffer in off design conditions, although chillers equipped with VFDs are significantly more efficient in off design operation than ones operating at constant speed [15].

2.4 Heat Pump Modeling

Many studies have attempted to quantify heat pump performance, but relatively few in the open literature have simulated transient conditions. Fewer still have been concerned with transients of heat pumps used to generate industrial process heat, and the combination of these with an ambient temperature source presents a totally unexplored area of research.

Many studies have attempted to quantify the performance of heat pumps, but relatively few in the open literature have investigated transient conditions through simulation. The authors found that previous investigators have largely been interested in either predicting the performance, usually the COP of the examined heat pump, at one or several operating points [16], [17], [18], [19], [20], [21], [22], [23], [24], [25], [26], [27], [28], [29], or simply quantifying the performance of a system through experimentation without prediction [30], [31], [32], [33], [34], [35], [36], [37], [38], [39], [40]. Of these above efforts which did attempt a prediction through modeling, none are a full system transient model; they did not look at controls dynamics or transient thermodynamic behavior of the working fluid throughout the system in startup or in the transition from full load to part load. Furthermore, none of these studies have been concerned with industrial process steam generation, dynamic compression, or controls optimization.

Existing transient studies of heat pumps have been concerned with space heating and hot water applications. These investigations have quantified system performance and dynamic behavior during startup [41], [42], [43], [44], long-term weather-dependent system performance of an air sourced hot water system [45], [46], [47], standalone compressor performance [48], hot water delivery temperatures [49], and integration of thermal storage in a cascade heat pump [50]. Other investigators have constructed a digital twin of a heat pump system based on real time operational data, but transient predictions from the model were not reported [51]. One constant

factor in the methodology of these studies is the use of custom-scripted mathematical models which are then computed using various solution methods. As system complexity increases, modeling systems in this way becomes cumbersome due to the number of equations that must be used to accurately describe the system's behavior. For the same reasons, it may also be difficult to use these types of models for extrapolation of system performance and behavior after modification.

Chamoun et al. conducted a transient study on an industrial single-stage twin screw compressor waste heat recovery heat pump [41]. The investigation is focused on an air purging system that eliminates air from the system at startup. The high side and low side pressures as well as the mass flow rate through the compressor were the main results of the investigation, but little else was presented in terms of data. The model was able to predict the movement of air through the system as it was purged during the startup sequence.

Chamoun et al. later published a transient study of a twin-screw water vapor compressor for heat pump applications [48]. This study mathematically modeled the transient thermodynamics of the compression process. The main results were the temperature and pressure evolutions along the compressor screws as a function of the rotational angle, with and without water injection. It was found that water injection would greatly improve the performance and reliability of the compressor.

Ndiaye et al. investigated the behavior of a single-stage reciprocating compressor geothermal space-heating heat pump. The study consisted of one duty cycle from startup to steady state operation and then to shutdown [42], [43]. The study consisted of a mathematical model of the heat pump system that was compared and validated with test data from the test prototype system. Results compared the model's prediction and the measured values from the prototype heat pump for the following quantities: compressor power, evaporation and condensation pressures,

source water inlet and outlet temperature and air inlet and outlet temperatures. The model performed well for startup and steady operating conditions but struggled to capture shutdown behavior due to leakage in one of the valves in the prototype.

Nenkaew et al. investigated a cascade-heat-pump hot-water heater system in startup and steady state operation for three different water flow rates [44]. The study was mostly concerned with the heat delivery rate, the top cycle compressor power over time, and top cycle COP. The purpose of this investigation was to determine the combined effects of different water flow rates and the changing sink temperature on the compressor power and system COP while the hot-water tank is heated.

Bellos et al. conducted a long-term transient study of an air sourced reciprocating compressor heat pump hot-water-heater [45]. The study used weather data from two different cities and manufacturer supplied compressor efficiency data to predict realistic yearly operating data. The model compared the performance of the heat pump with an oil boiler and found that the heat pump had a reasonable payback time, was cheaper to operate, and produced less CO2 than the oil boiler.

Zamojski et al. modeled the behavior of a heat pump hot-water-heater's condenser [49]. This study derived ordinary differential equations for control volumes representing the condenser. The model was compared to operating data taken from a commercially available hat pump. The model was able to predict the refrigerant and water outlet temperatures for a single operating point.

One constant factor in the methodology of these predictive modeling studies is the use of custom-scripted mathematical models which are then computed using various solution methods. The scope of these models is ultimately limited by the size of the systems of equations required to

describe the system, and the time it takes to input them into a solver. Unlike these models, specialized software tools provide much greater leverage as model complexity increases due to their automation of many labor-intensive parts of mathematical modeling and equation solving. Conversely, this work presents an investigation of a high temperature, high lift, ambient sourced heat pump both in startup and load following transient conditions using a specialized software tool optimized for thermal systems modeling, the combination of which is totally absent from the open literature.

2.5 Chiller Transient Modeling

While there has been little research in full system transient simulation of high-lift centrifugal compression heat pump systems, there has been significant research in the transient behavior of centrifugal chillers in startup and other transient conditions.

Okazaki et al. developed a rigorous mathematical model of a centrifugal chiller with the goal of optimizing the startup process [52]. The study uses advanced mathematical programming techniques to solve differential equations representing the states of the working fluid. The study results in an optimized startup process for the compressor and control valves of the chiller.

Schalbart et al. simulated a centrifugal chiller in quick startup [53]. Mass energy and momentum balances were applied to the discretized representations of the system, and a PD controller was used on the expansion valve. The study resulted in an improved control scheme during startup which actuates the expansion valve to avoid both liquid ingestion to the compressor and compressor surge.

Li, Li et al. created a transient model of a centrifugal chiller using Modelica [54]. A Lyapunov based nonlinear stability analysis was applied to the model for the purpose of proving the stability of a proposed control scheme for avoiding compressor surge.

Browne et al. used a mathematical model to predict the performance of a centrifugal vapor compression chiller during startup and successive steady state operation, and in transitioning from full load to part load [55]. The model resulted in a prediction of performance and operating state points that matched well with the measured test data.

Zhang et al. developed a transient mathematical model of a screw chiller and validated the results with a test prototype chiller [56]. The model was able to match the behavior of the prototype well, but both the model and the prototype showed inopportune expansion valve performance. Zhang followed up with another study which used the model to compare prospective control strategies [57].

As with transient studies of heat pumps these studies use custom-scripted mathematical models computed in a variety of ways, and naturally the limitations of increasing complexity still apply. Accordingly, none of these models are used to extrapolate system performance after a component replacement.

2.6 Modeling Software

The use of advanced software tools offers the potential to model much more complex systems by streamlining the modeling process both by using model templates and recommendations for mitigating issues like solver nonconvergence and unreasonable simulation solve-time problems. Controls design benefits especially from the use of modeling software tools. These tools provide a fast and easy way to test new control strategies and offer options for

algorithmic tuning of controller gains further simplifying the modeling process. They also allow for easier sensitivity analysis of how a change to a component or the system configuration will affect operation. Additionally, the use of commercial software leverages robust and already proven component models which have already been tested and validated against other systems which allows for greater focus on system level modeling of this novel thermodynamic cycle.

2.7 GT-SUITE System Modeling

The GT-SUITE modeling environment is a Multiphysics differential equation-based simulation environment which allows for transient system modeling of a wide range of physical systems. While studies using GT-SUITE to model high temperature heat pumps are not available in the open literature, investigations have been published using it to model other similar thermal systems.

Several studies have been published by a research group from Tianjin university using GT-SUITE to model wase heat recovery systems for diesel trucks [58], [59], [60], [61], [62]. These studies all use the standard GT-SUITE modeling process which involves calibrating individual components to match measured or expected performance before they are integrated into the larger system model. These studies along with one publication highlighted by Gamma Technologies [63], do however represent the extent of the peer-reviewed open literature found by the authors that use GT-SUITE for thermal systems modeling.

Zhao et al. investigated the performance of a heavy-duty truck engine fitted with an organic Rankine cycle waste heat recovery system [58]. The study was conducted only in GT-SUITE; however, it was followed by a series of papers from the same research group which investigate the performance of a transcritical CO2 Rankine power cycle in GT-SUITE that includes experimental validation of the model which is discussed below.

Shi et al. and Li et al. built and tested a transcritical-CO2-power-cycle waste-heat-recovery system for a diesel truck engine [59], [60], [61]. The test bench first utilized an expansion valve in place of the turbine because the custom turbomachinery was still in the design phase. The authors hoped to use data from this test setup to aid in the turbine's design process.

Li et al. then constructed a model of the transcritical-CO2-power-cycle waste-heat-recovery system in GT-SUITE [62]. The model was calibrated to match the measured performance of the test prototype system which had an expansion valve installed in place of the turbine. Once the model had been calibrated, it was then used to extrapolate the theoretical performance of the system once the turbine had been installed.

These studies all use the standard GT-SUITE modeling process which involves calibrating individual components to measured-data or expected performance before they are integrated into the larger system model. Gamma Technologies also highlights several high-level commercial publications and one peer reviewed article outlining how GT-SUITE has been used to model thermal systems and has commonly been used for modeling heat pump systems for use in electric vehicle climate control systems, geothermal heat pumps and hot water heaters [63], [64], [65], [66].

2.8 Deficiencies in Literature

As outlined in the literature review above, and Table 2-1, those studies that have investigated transient behavior have been conducted on heat pumps that require waste heat, produce only hot water and/or use a positive displacement compressor rather than a centrifugal compressor. More specifically, no study was found by the authors in the open literature which investigates system operational dynamics of an ambient-temperature-source Turbo-compression driven steam-generating heat pump with steam delivery temperature of 150°C, and no study has investigated the

system behavior when transitioning from full load operation to part load operation of high temperature heat pumps more generally.

Table 2-1: Current literature on heat pump/chiller full system transient modeling

Study	Application	Compressor type	Heat source	Cascade?	Startup?	Load following?
Chamoun et al. [41]	Hot water	Twin screw	Waste	No	Yes	No
Ndiaye et al. [42], [43]	Space Heating	Reciprocating	Geothermal	No	Yes	No
Nenkaew et al. [44]	Hot water	Not listed	Chilled water	Yes	Yes	No
Bellos et al. [45]	Hot water	Reciprocating	Ambient air	No	No	Yes
Zamojski et al. [49]	Hot water	Not listed	Ambient air	No	No	No
Okazaki et al. [52]	Chiller	Centrifugal	Chilled water	No	Yes	No
Schalbart et al. [53]	Chiller	Centrifugal	Chilled water	No	Yes	No
Li, Li et al. [54]	Chiller	Centrifugal	Chilled water	No	Yes	Yes
Browne et al. [55]	Chiller	Centrifugal	Chilled water	No	Yes	Yes
Zhang et al.[56], [57]	Chiller	Screw	Chilled water	No	No	Yes
Current Work	Process Steam	Centrifugal	Ambient air	Yes	Yes	Yes

This thesis will address the stated deficiency in the literature by constructing a transient thermodynamic model of the heat pump system based on manufacturer supplied component performance data that is able to match the performance of the test prototype system.

CHAPTER 3: Methodology

This work aims to present a transient thermodynamic model of a centrifugal-compression-driven, ambient heat sourced, cascade configuration, steam generating heat pump system using the GT-SUITE software environment. The air source heat exchanger was not modeled as part of this study since it is not directly coupled to the heat pump cycle. Instead, 15°C glycol/water solution was assumed as the heat source. In the physical system, the glycol loop would be coupled to an air-to-glycol heat exchanger which would supply the 15°C glycol/water heat source at an ambient air temperature of about 25°C. The model matches the configuration of the test prototype heat pump constructed at the Colorado State University Powerhouse Energy Campus.

Table 3-1: Heat Pump Component List

Component	Description
HX-110 (BKU)	Top cycle condenser/steam boiler, bonnet-kettle-u-tube (BKU) type
HX-130 (SLHX)	Top cycle suction line heat exchanger
HX-140	Inter-cycle heat exchanger, bottom cycle condenser/top cycle evaporator
HX-240	Bottom cycle evaporator
C-100	Top cycle low pressure compressor (two stages, LP-1 and LP-2)
C-101	Top cycle high pressure compressor (two stages, HP-1 and HP-2)
C-200	Bottom cycle compressor (two stages)
EV-140	Top cycle electronic expansion valve
EV-240	Bottom cycle electronic expansion valve
RCVR-210	bottom cycle receiver drum
RCVR-110	Top cycle receiver drum
Piping Legs	piping connections between components includes elevation change and losses due to fluid friction and bends.

3.1 Heat Pump Model Configuration

A process flow diagram of the system evaluated in this work is provided in Figure 3-1. The heat pump design consisted of two vapor compression cycles in a cascade arrangement. The bottom cycle used refrigerant R513a, a brazed plate evaporator, a brazed plate condenser, an

electronically controlled expansion valve, and an off-the-shelf, two-stage refrigerant compressor. The top cycle used refrigerant R1233zd(E), a brazed plate evaporator (which also functions as the bottom cycle condenser), a shell-and-tube kettle-type condenser, a brazed plate suction line heat exchanger (SLHX), and two, two-stage, refrigerant-cooled-ball-bearing, single-shaft compressors fabricated in-house.

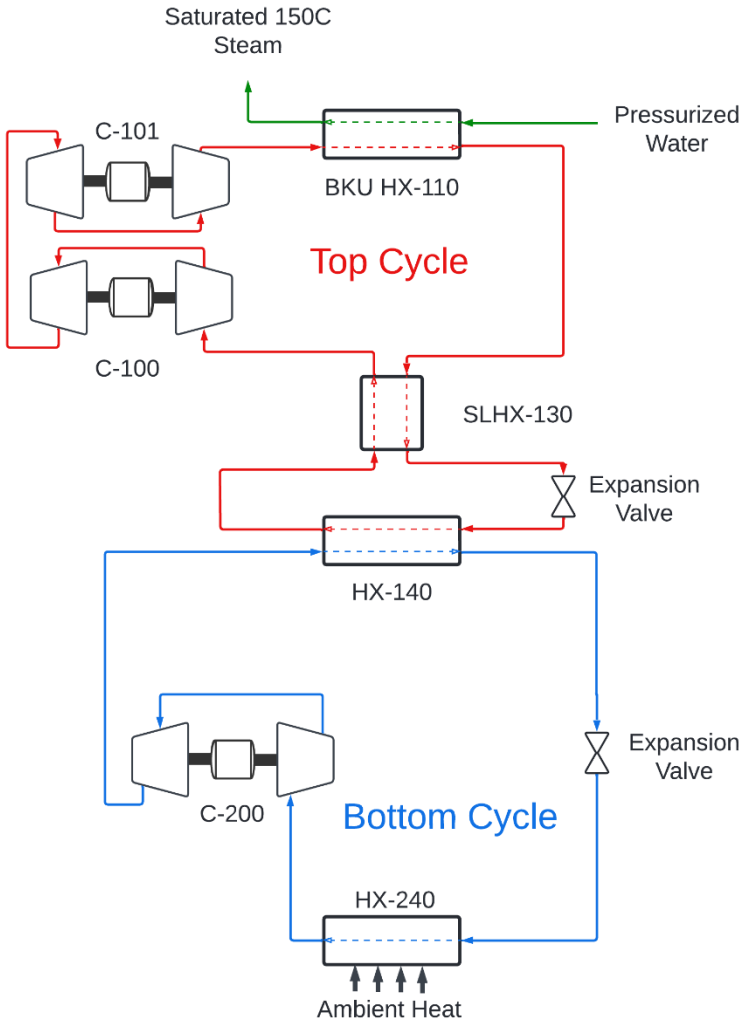

Figure 3-1: Heat pump process flow diagram (PFD)

The refrigerant in the bottom cycle was first boiled in HX-240 by absorbing heat from a 15°C glycol stream which, in turn, absorbed heat from the air. The refrigerant vapor was then compressed by the bottom cycle compressor before moving to the middle heat exchanger where it condensed and exchanged heat with the top cycle refrigerant. The bottom cycle refrigerant was then expanded across the electronic expansion valve before beginning the cycle again. The top cycle of the cascade followed the same configuration as the bottom cycle but with one key difference. The top cycle incorporated an SLHX where subcooled liquid exiting the condenser provided heat to the superheated vapor exiting the evaporator. The SLHX improved the COP of the top cycle by further subcooling the liquid leaving the condenser before it was expanded through the expansion valve. This shifted the expansion process to the left of the P-h diagram, which resulted in a larger fraction of the two-phase mixture being liquid after expansion. Because of this lower vapor quality, more heat was transferred through boiling the refrigerant instead of superheating it, providing greater isothermal heat transfer. The heat removed from the refrigerant in the liquid stream was then returned to the refrigerant in the gas phase stream after it passed through the evaporator. In addition to the thermodynamic benefits, the SLHX also provides liquid ingestion protection to the compressor by superheating the vapor prior to entering the compressor. It is important to avoid liquid ingestion because liquid droplets can damage the high-speed compressor rotor due to their much higher density compared to that of vapor.

3.2 Heat Pump Steady-State Model

An initial steady-state model of the desired thermodynamic cycle was created in Engineering Equation solver (EES). This model was used to establish the desired state points of the working fluid throughout the system. Components were then sized to meet the operating conditions specified by the steady-state thermodynamic model. The steady state model acted as a

baseline for comparison and evaluation of both the transient model and the prototype test because it outlines the desired thermodynamic cycle.

Table 3-2: EES modeling assumptions – compressors

Machine Name	Isentropic Efficiency [%]	Pressure Ratio [-]
Bottom Cycle stage 1	76.7	2.29
Bottom Cycle stage 2	76.7	2.29
Top Cycle LP stage 1	81.5	1.879
Top Cycle LP stage 2	79.5	1.631
Top Cycle HP stage 1	80.8	1.662
Top Cycle HP stage 2	79.0	1.603

Table 3-3: EES modeling assumptions – heat exchangers

Heat Exchanger Name	Outlet SC/SH target or UA	Operating Pressure [kPa]
HX-240	5°C SH	398.7
HX-140 (TC)	5°C SH	392.2
HX-140 (BC)	1.5°C SC	1972
HX-130-SLHX	3.757 kW/K	2888 liq/388 vap
HX-110-BKU	3°C SC	2969

Table 3-4: Heat-source and heat-sink boundary conditions

Fluid	Flow rate [kg/s]	Inlet/Outlet Conditions
Feedwater/Steam	0.3063	145°C in/150°C out
EG-W 50%	13.56	15°C in/9°C out

3.2.1 Steady State Energy Balance and Equations

The isentropic efficiency, shown in Equation 3, was used to determine the outlet enthalpy and thus outlet temperature of the refrigerant after compression between two given pressures.

$$\eta_s = \frac{h_{2,s} - h_1}{h_2 - h_1} \tag{3}$$

The quality of the refrigerant after expansion through the EXV was determined according to an adiabatic expansion via a table lookup using the enthalpy of the refrigerant entering the valve and the pressure at the valve outlet to determine the outlet quality.

The outlet temperatures of the fluids in a heat exchanger were determined by energy balance using Equations 4, 5, and 6. The heat rates from each side of each exchanger must equal each other, along with specified superheat and subcooling targets at the outlet of the exchangers. A *UA* value was used for the SLHX, representing both the heat exchanger area *A*, multiplied by the overall heat transfer coefficient *U*, represented as a single number. The total desired steam production heat-rate from HX-110 was specified to be 650 kW.

$$\dot{Q} = \dot{m} * (h_{out} - h_{in}) \tag{4}$$

$$\dot{Q} = UA * (LMTD) \tag{5}$$

$$LMTD = \frac{(T_{hot,in} - T_{cold,out}) - (T_{hot,out} - T_{cold,in})}{\ln\left(\frac{T_{hot,in} - T_{cold,out}}{T_{hot,out} - T_{cold,in}}\right)} \tag{6}$$

Pressure drop in the heat exchangers was determined using manufacturer data for components purchased for use in the physical prototype and the desired operating pressures in each component.

3.3 GT-SUITE Modeling Process

The process of modeling a system in GT-SUITE begins with calibrating component models of various types on standalone virtual test benches using performance data and geometric specifications. The performance data can be obtained through various means including laboratory testing, manufacturer supplied performance data and/or using additional Computational Fluid Dynamics (CFD) or heat exchanger design and analysis software. The use of empirically collected data is preferred but is not always practicable early in the research and development process, especially when the goal of the model is performance prediction. Once each of the components has been calibrated as desired, they can be imported into a larger model. Entire models can also be imported into other models, which allows for subsystem testing and optimization before integration. In this work, components were calibrated to match expected performance of those installed on the prototype test system using expected performance data.

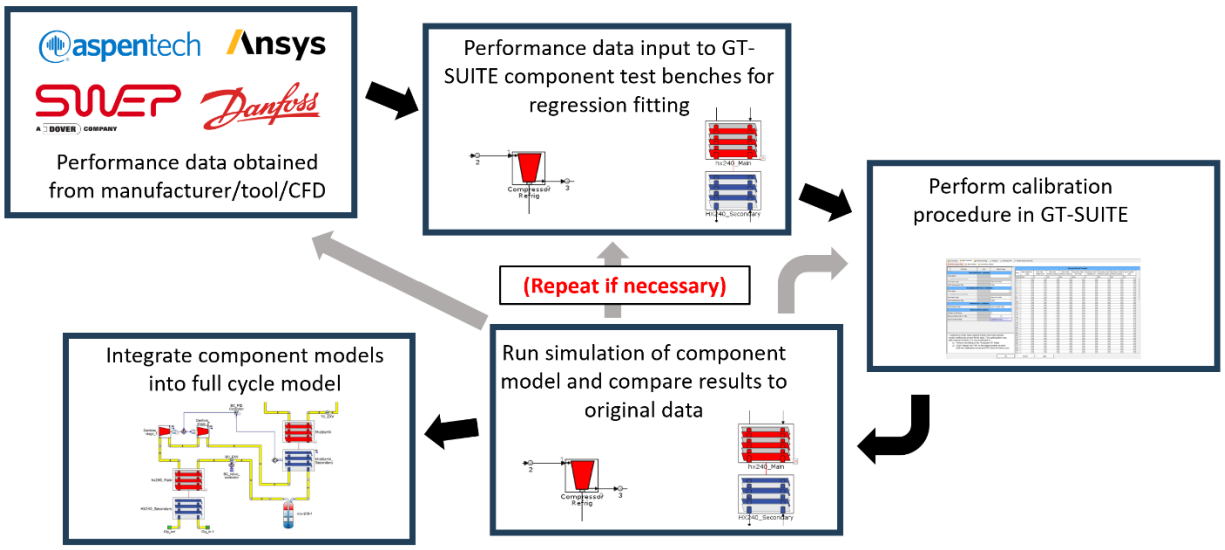

Figure 3-2: GT-SUITE component calibration process flow chart

3.3.1 Heat Exchanger Modeling

GT-SUITE heat exchanger calibration works by utilizing tabulated heat exchanger performance data as an input and automatically regression-fits coefficients and exponents of the relevant heat transfer correlation selected by the user to match the prediction with the tabulated data. After this initial calibration is completed successfully, the fitted heat transfer correlations are used, and the tabulated data is no longer referenced. This calibration process is computationally expensive up front, but once the component model is integrated into a system model, it offers much greater savings in computational time. Calibration data must include the inlet and outlet state of each fluid, the flow rate of each fluid, and the total heat duty exchanged between the two. Geometric data for the plate spacing, distributor type, and port size are also defined along with the exchanger material.

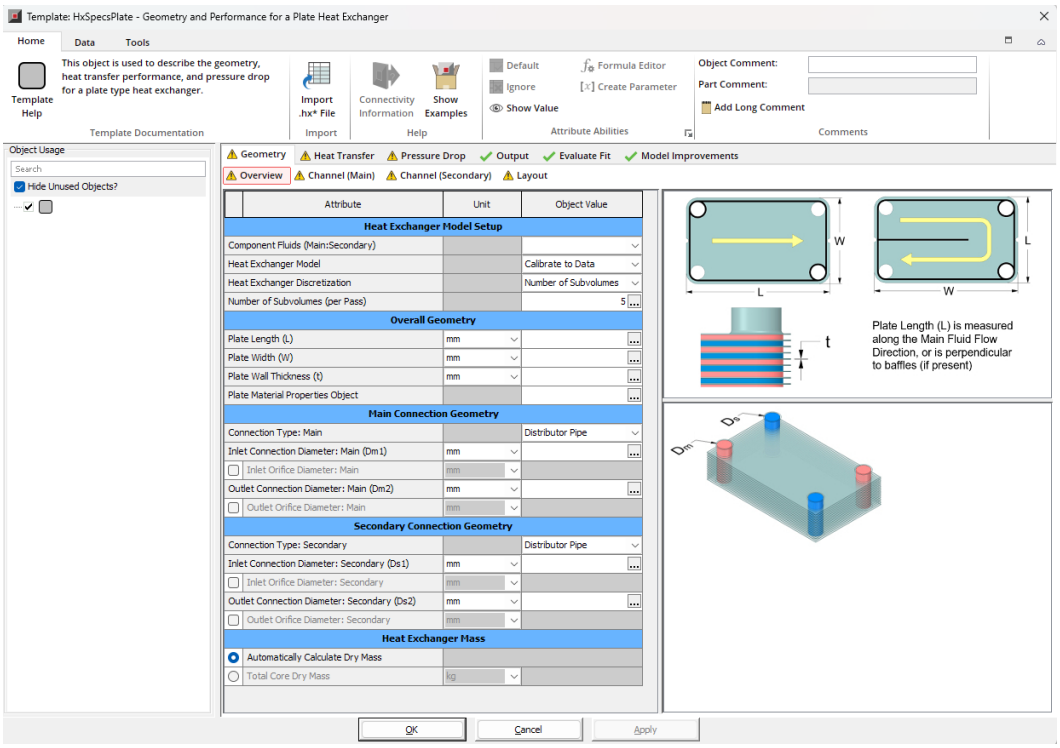

Figure 3-3: GT-SUITE heat exchanger specifications object interface for plate type

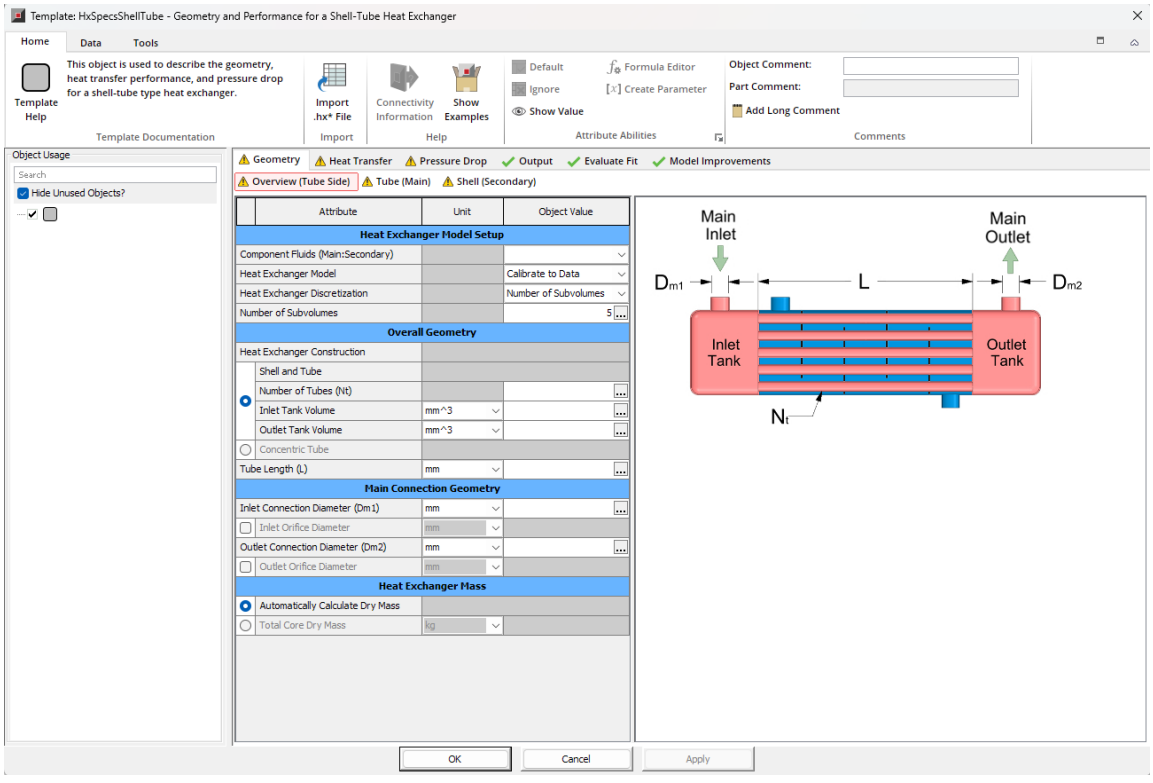

Figure 3-4: GT-SUITE heat exchanger specifications object interface for shell-and-tube type

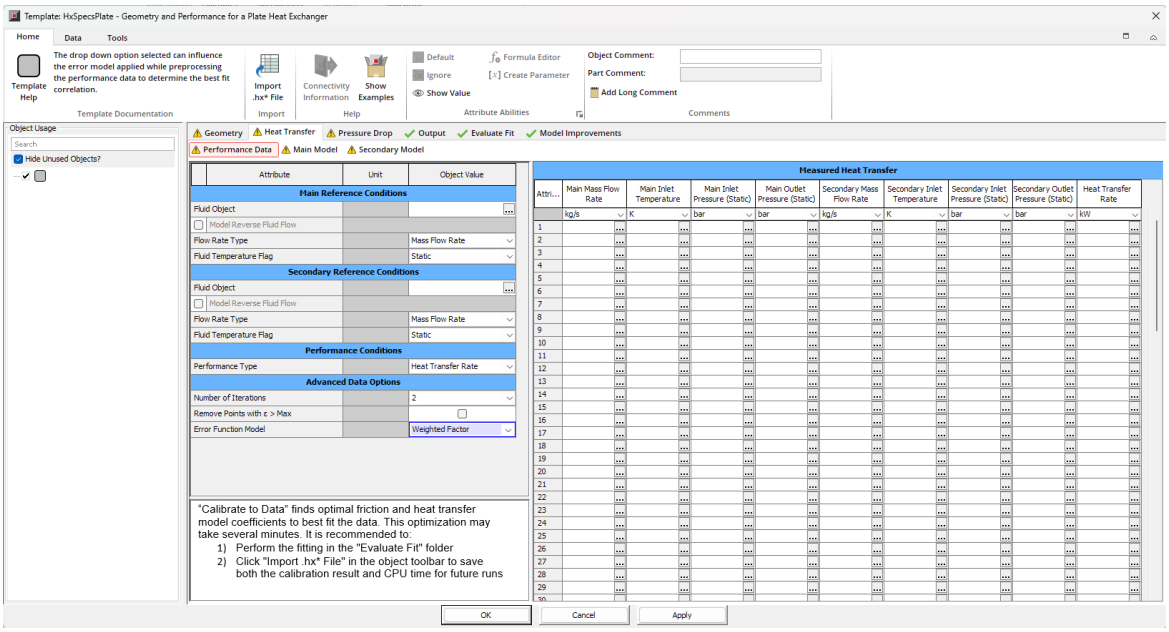

Figure 3-5: GT-SUITE heat exchanger specifications object heat transfer data inputs

All heat exchanger components were calibrated with performance data generated from Aspen Exchanger Design and Rating using the heat exchanger geometry provided by the manufacturer. The correlations recommended by GT were used in all exchangers. The relative error of mass flow, pressure drop and heat duty in each heat exchanger component was within 2% of the provided data after calibration. The heat plate type heat exchanger object template was used for all exchangers except HX-110 which was modeled using the shell and tube template. The average relative error of primary and secondary pressure drops as well as heat transfer rate in each heat exchanger component as compared to the original performance data is reported in Table 3-5.

Table 3-5: Heat exchanger calibration results

Exchanger Name	Primary ΔP error [%]	Secondary ΔP error [%]	Heat Transfer Rate Error [%]
HX-110-BKU	0.381	0.986	0.264
HX-130-SLHX	0.174	0.688	0.055
HX-140	1.086	1.819	0.914
HX-240	0.750	1.141	0.368

3.3.2 Compressor Modeling

The refrigerant compressor object in GT-SUITE used a direct table lookup of the performance map with linear interpolation between tabulated values. The refrigerant used to generate the performance map is specified alongside the tabulated data. If a different refrigerant than the one provided with the map is used in the model, GT-SUITE will adjust the performance values based on the differing densities between the two refrigerants. It should be noted that this method can only be applied if the two refrigerants have similar fluid properties.

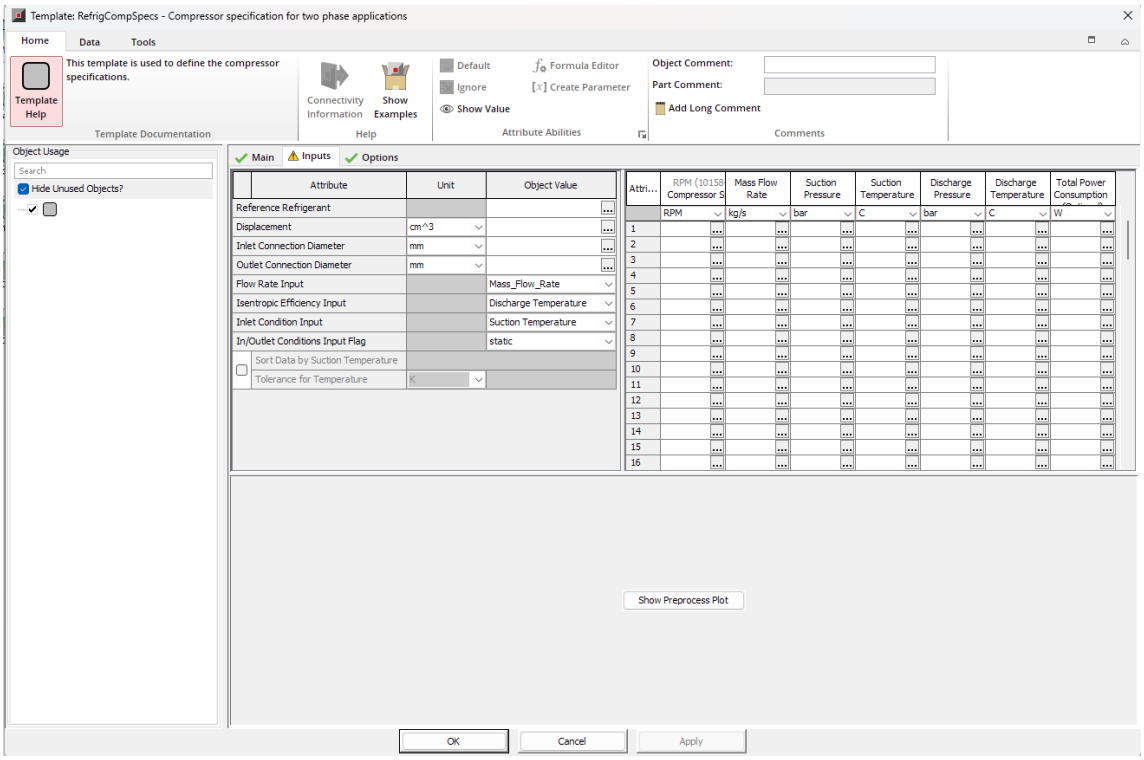

Figure 3-6: GT-SUITE refrigerant compressor specifications object

Performance maps for the in-house designed and fabricated top cycle compressors were generated using Ansys CFX. These performance maps were then provided to the compressor component object. Performance of each compressors model was then verified, with relative errors between the compressor map data and the simulation output reported in Table 3-6.

The performance map for the Danfoss Turbocor compressor was provided by Danfoss for use with R134a. Because the compressor is being used with R513a instead of R134a, it was expected to have a somewhat larger error for the mass flow rate through the compressor as compared to the map because of the differing molecular weight of the two refrigerants. The Danfoss compressor object calibration relative errors as compared to the original map data are reported in Table 3-7.

Table 3-6: Top cycle compressor calibration results

Compressor name	Mass flow error [%]	Pressure ratio error [%]	Efficiency error [%]
C-100-A	0.017	0.005	0.035
C-100-B	0.359	2.733E-6	0.072
C-101-A	0.038	0.001	0.033
C-101-B	0.501	0.001	0.06

Table 3-7: Bottom cycle compressor calibration results

Compressor Name	Mass flow error [%]	Pressure ratio error [%]	Discharge temperature error [%]
C-200-A	6.670	0.626	0.703
C-200-B	7.614	2.162E-6	0.691

A compressor map can also be used as a visualization tool for determining how well a gas compressor is performing. A compressor's map depicts the mass flow rate of a compressor corrected for the effects of suction pressure on suction density and volumetric flow rate, the pressure ratio, the efficiency, and the machine speed. The operational region of the compressors is defined between its 'surge line' (left edge) and 'choke line'(right edge). The surge line defines the maximum pressure ratio for a given speed before the onset of a flow reversal condition known as surging or stalling [9]. The choke line defines the maximum amount of flow a machine can output,

governed by the Mach number reaching unity somewhere in the machine [9]. Many speeds lines are included on a single map, and each operational point also has corresponding efficiency. Lines of constant efficiency are plotted between the stall and choke lines on the compressor map as shown in Figure 3-6.

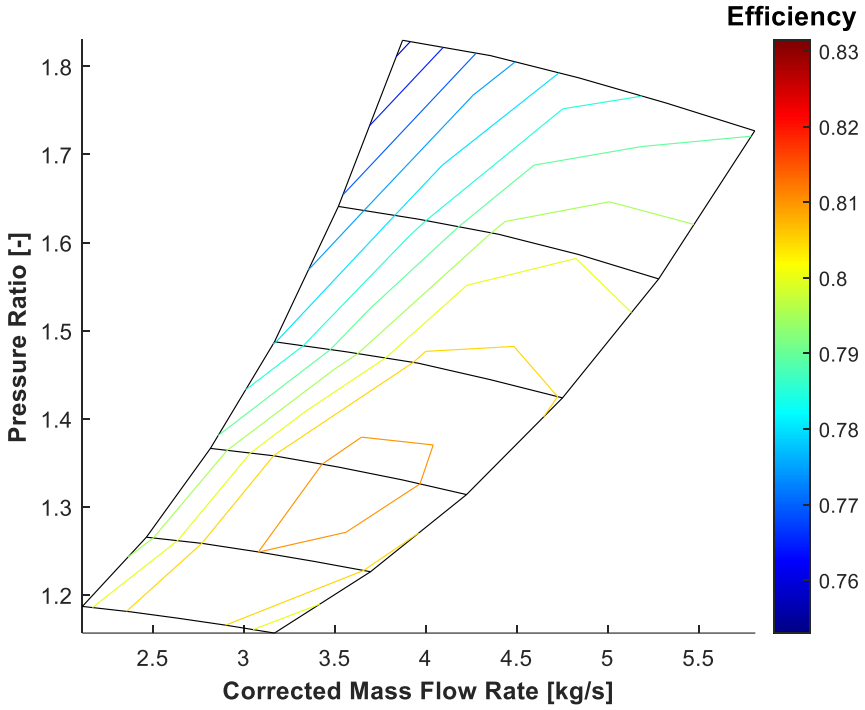

Figure 3-7: Compressor Map Example

A compressor is a volumetric machine. Ultimately it operates on aerodynamic, flow-velocity based principles. As such differences in suction pressure are accompanied by differences in suction density, resulting in a different flow velocity for a given mass flow rate. A compressor map is generated for a given suction condition, and as such the mass flow rate must be adjusted to account for the difference in operational suction pressure from that of the map. Mass flow rate was corrected using Equation 7. Compressor map graphics were created independently in MATLAB using operation data from GT-SUITE.

$$\dot{m}_{corr} = \frac{\dot{m}_{op} * \sqrt{T_{op}} * P_{ref}}{P_{op} * \sqrt{T_{ref}}} \quad (7)$$

3.4 Expansion Valve Modeling

The expansion valve model required inputs of the type of target property the valve is trying to meet (super heat, quality, or enthalpy), the value of the target property, the object where the target variable is to be sensed, the maximum and minimum orifice area, the initial area, and a time constant for the speed of actuation. The expansion valve object used a built-in PID controller to meet the desired setpoint. These expansion valve inputs are critical parameters for calibrating the system model. The values used for each expansion valve are reported in Table 3-8.

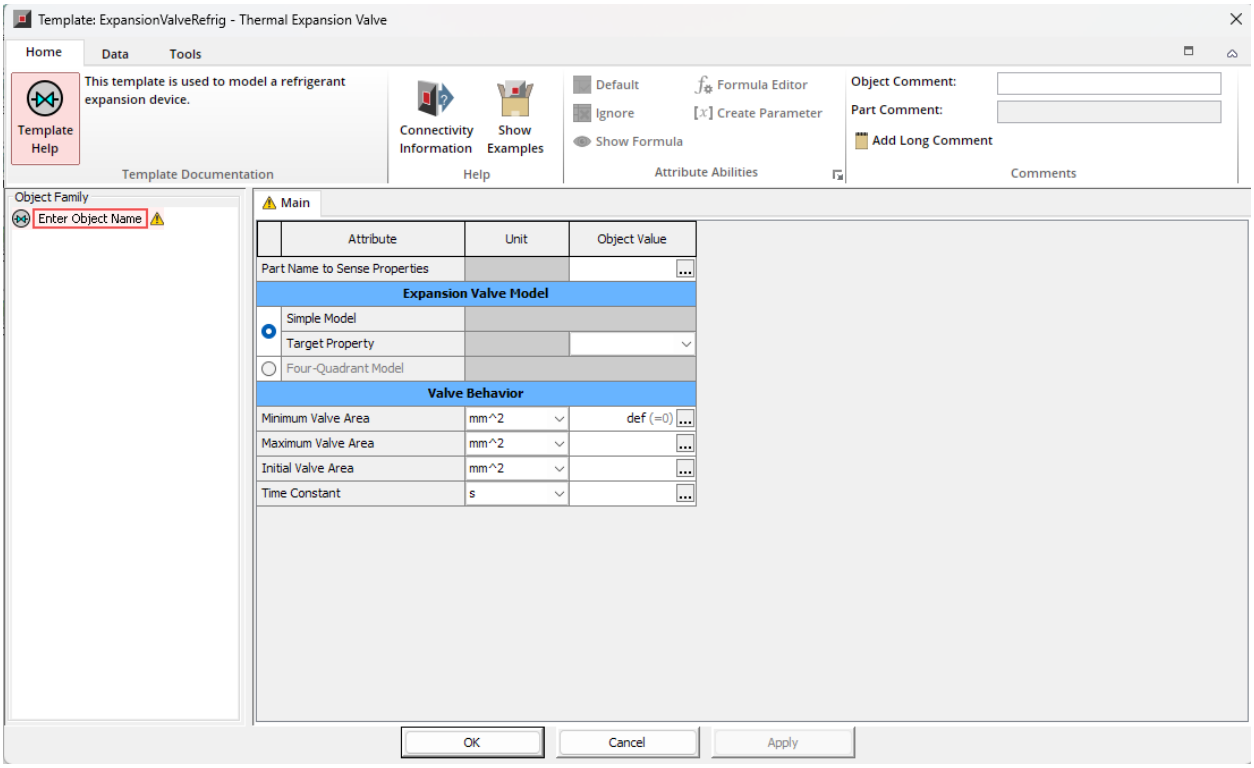

Figure 3-8: GT-SUTE expansion valve object interface

Table 3-8: Expansion valve inputs

Valve Name	Target SH	Sensor Location	Max Area [mm^2]	Min Area [mm^2]	Initial Area [mm^2]	Time Constant [s]
EV-240	5 K	HX-240 outlet	65	15	15	70
EV-140	5 K	HX-140 evaporator outlet	68	15	15	65

3.4.1 System Integration

After each component was calibrated, separate models of the top and bottom cycles were created, and preliminary simulations were run with constant compressor speed and expansion valve superheat target to diagnose and mitigate any initial errors and slow-running models.

Many issues were encountered through the integration process including errors in piping geometry, REFPROP version issues, flow volume discretization issues, compressor map data issues, and disadvantageous initial conditions all of which were diagnosed and corrected using information from the console messaging and support from Gamma Technologies.

Once the simulation behavior and computation duration of the individual top and bottom cycle models were acceptable, they were combined into a full cascade-cycle model, pictured in Figure 3-8. This full cycle model was successively run with constant compressor speed and expansion valve superheat-target to confirm that the behavior of the combined cascade cycle matched that of the individual cycles.

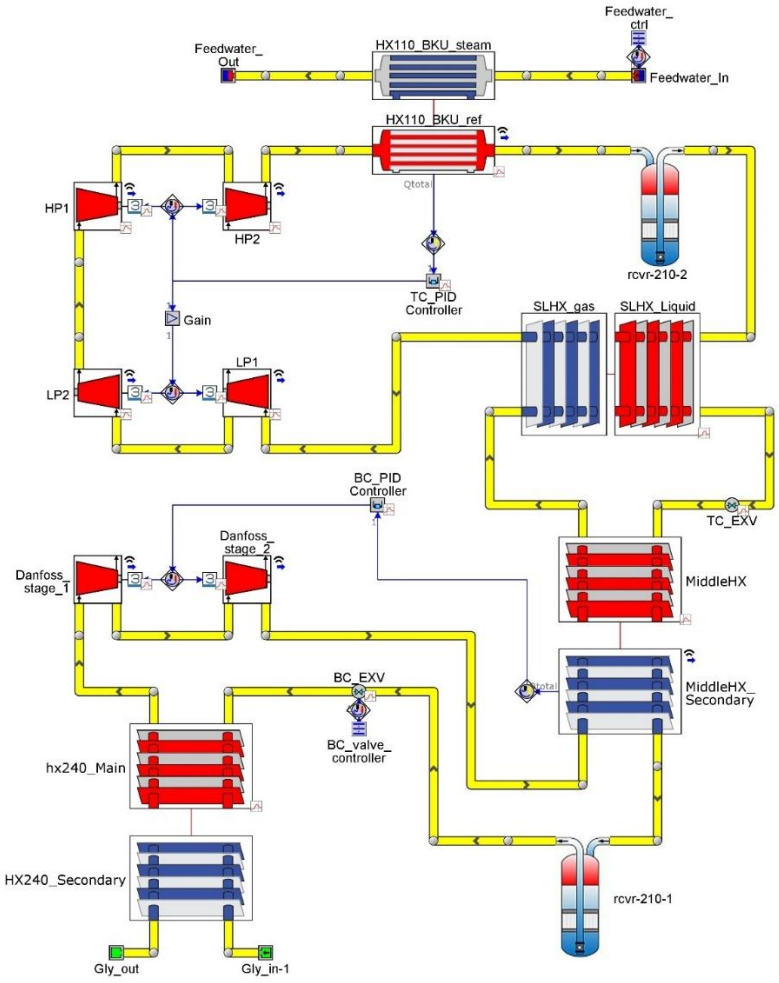

Figure 3-9: GT-SUITE model schematic

3.4.2 Refrigerant Charge Optimization

Proper refrigerant charge is essential to achieving the desired thermodynamic states at various points in the cycle. Too much charge results in more of the system being in the liquid phase than desired, and too little causes more of the system to be in the gas phase than desired. This being the case, multiple simulations were run across an array of charge values to determine the correct charge based on the subcooling of the refrigerant exiting the condenser in its respective cycle. The integrated cycle model was used to determine the refrigerant charge. First the top cycle charge was

determined, then the bottom cycle. After confirmation that the steady state performance of both the top and bottom cycles in the model matched the expected cycle state points, transient system operation was introduced. Realistic piping lengths and elevation changes were later added to the model and the charge was adjusted accordingly. This was necessary due to changes in the ratio of the volume of liquid full pipes to the volume of vapor full pipes during steady state operation.

3.4.3 Modeling Transient Conditions

The main system control variables of the heat pump were the speed of the compressors and the opening percentage of the expansion valves. Both the valves and compressors were controlled using PID controllers. The EXV object had a built-in PID controller and thus was always controlled in this way. The compressors were controlled using a generic PID controller object provided in GT-SUITE. The drivers of transient conditions in the model were a cold startup condition, a changing steam demand, and a changing outdoor temperature. The controllers were tuned through in an iterative process to achieve stable operation and low settling time.

Table 3-9: GT-SUITE full system model input parameters

Parameter	Value
Glycol flow rate	14.18 kg/s
Boiler feedwater flow rate	0.306 kg/s (0.258 kg/s)
Top cycle refrigerant charge density	288 kg/m^3
Bottom cycle refrigerant charge	315 kg/m^3
Top cycle design speed - HP	27,600 RPM
Top cycle design speed - LP	24,900 RPM

3.5 Preliminary validation

An important part of any modeling effort is validation of the model's predictions against a physical prototype to prove that the predictions of the model match reality. This can be challenging when a model and prototype are being constructed in parallel, or if the model is intended to help inform design decisions before completion of the prototype. In this work the model and prototype were constructed in parallel, so prototype operational data was not immediately available. The modeling process used in this work does, however, provide a level of preliminary validation for the model. The steady state model of the system was used in the design of the physical prototype, and as such the system components were sized to provide the desired performance outlined in the EES model. Performance data for the brazed plate heat exchangers was obtained from the SWEP heat exchanger sizing tool used in conjunction with Aspen EDR, and data for HX-110 was obtained using manufacturer supplied geometry data in Aspen EDR, ensuring that the predicted performance of the heat exchangers in the GT-SUITE model is realistic. Performance data from the Danfoss compressor was obtained from Danfoss and operational data from the model was fed back into the Danfoss OEM performance tool to ensure realistic compressors operation. C-100 and C-101 maps were generated in Ansys CFX from the same CFD model that was used to design the compressors wheels. By using commercial products like Aspen EDR, Ansys CFX, and the SWEP heat exchanger tool and comparing the results of the GT-SUITE model to the steady state model used in the system designs, a level of intrinsic validation was built into the model through leveraging prior validation work done in development of those commercial tools.

CHAPTER 4: Results and Discussion

4.1 Transient Model Preliminary Validation with Steady State Model

Steady state results of the GT-SUITE model were compared with data from EES to confirm that each vapor compression cycle behaves as expected, and the model has been correctly configured. This comparison was made by overlaying the cycle state point from both EES and GT-SUITE onto the P-h and T-s diagrams of the vapor dome of each refrigerant for a direct comparison. The total refrigerant charge was a significant factor in achieving the desired vapor compression cycle state points. The optimal refrigerant charge was determined by running multiple simulation cases with a spread of values for the total refrigerant mass, which was achieved by varying the average system density parameter. Subcooling of the refrigerant exiting the condenser was used as the optimization target for each cycle. The EES model subcooling values from Table 3-3 were used as targets. There was good agreement between the results from EES and GT-SUITE for steady state operation at the design point, after the charge optimization.

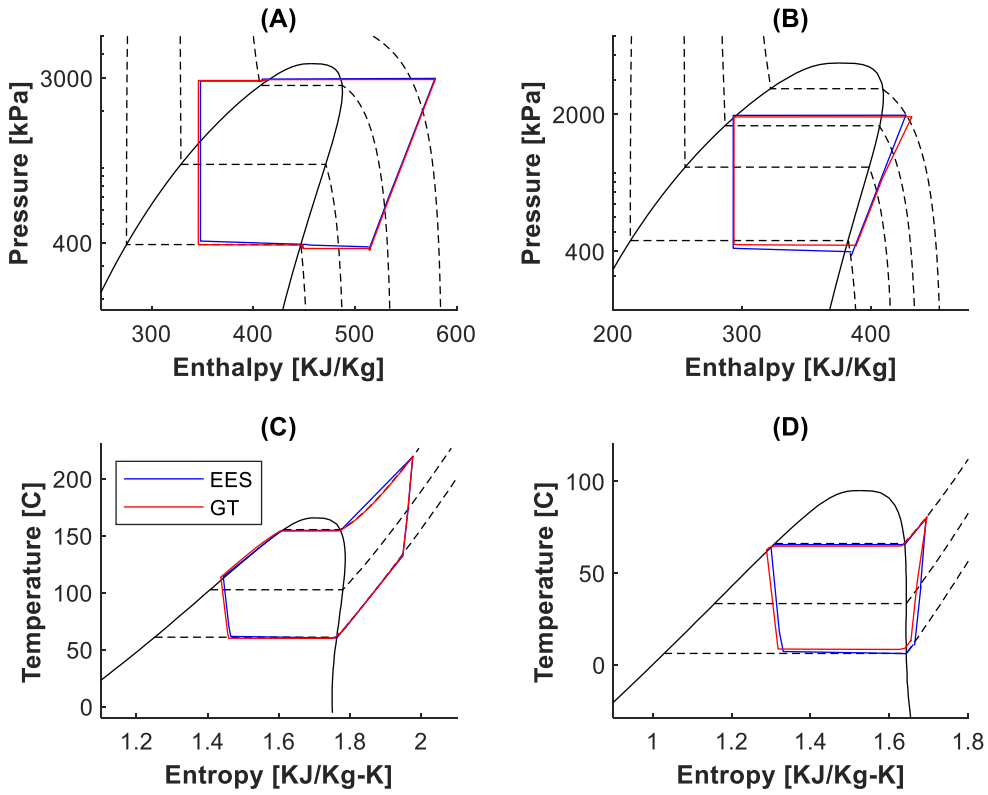

Figure 4-1: Comparison of cycle operating points. **(A)** - Top cycle *P-h* diagram, **(B)** - Bottom cycle *P-h* diagram, **(C)** - Top cycle *T-s* diagram, **(D)** Bottom Cycle *T-s* diagram

As shown in Figure 4-1, The bottom left corner of each cycle diagram begins with the refrigerant as a two-phase mixture entering the evaporator of its respective cycle. The refrigerant then moves around the cycle diagram in a counterclockwise direction, first being boiled at constant temperature and pressure along the bottom of each diagram and then being superheated along the dashed isobars and isotherms. The boiling pressures for the top and bottom cycles were 392 kPa and 398 kPa respectively. The top cycle refrigerant was superheated much more (75 K) than in the bottom cycle (5 K) due to the use of the SLHX. This provided both performance benefits and prevented the compressor from ingesting liquid during operational transients. The compression

process is represented on the right-hand side of each diagram. As shown in the T-s Diagrams in Figure 4-1 (C) and (D) the isentropic efficiency of the compression process resulted in a deviation from a vertical line, with vertical being an isentropic, or reversible compression. After compression, the refrigerant vapors were cooled, condensed and subcooled along the top of the diagram. The condensing pressures were 2940 kPa and 1940 kPa for the top and bottom cycle respectively. The top cycle refrigerant was subcooled much more (40K) than the bottom cycle refrigerant (2 K), again due to the SLHX. The refrigerant finally undergoes an isenthalpic expansion across the expansion valves of each cycle, represented by the vertical lines on the left side of the diagram. This returned the refrigerant to its original state as a two-phase liquid and the cycle begins again.

4.2 Compressor Control

PID controllers were implemented to control the speed of the compressors based on the desired steam heat-load from HX-110, of 650 kW and the desired heat transfer rate in HX-140 of 400 kW. The GT-SUITE PID controller can use manually entered gains or automatically calculated gains based on slope of response and settling time. The automatically calculated gain feature was selected in this work. The inputs of the controller were iteratively adjusted to achieve the desired operation. In the top cycle, the high-pressure and low-pressure compressors operate at different speeds. The HP compressor design speed was 27,600 RPM and the LP compressor design speed was 24,900 RPM. The compressor controller controlled the speed of the high-pressure machine, and the speed ratio between the low pressure and high-pressure compressor in the top cycle was held constant at the design point by applying a proportional gain of (24.9/27.6) to the control signal before it was passed to the low-pressure machine. The controller for the bottom cycle compressor controlled the heat rate in the middle heat exchanger, and the ratio of the set point of the heat rate

of HX-110 and HX-140 was held constant at the design point. At full load, the compressor controller settled on the design speed of 27,600 RPM for the top cycle machine, which corresponded to the design speed of 24900 RPM for the bottom cycle machine at the design condition of 650 kW in HX-110. The bottom cycle controller settled on a speed of 35,350 RPM the design condition of 400 kW in HX-140.

4.3 Compressor Transition to Turn-down and Back to Full-Load

The performance of the controllers was first verified at steady state at the design point without a startup or turndown transient. Next the steady state performance was confirmed at the turndown condition. After verification, a transient turndown condition was modeled by stepping down the requested HX-110 heat load from the boiler kettle from 650 kW to 550 kW during operation.

Figure 4-2 shows the inputs, outputs, and targets of the compressor PID controllers for the top and bottom cycles. Table 4-1 lists the name and number of events labeled in Figures 4-2 through 4-5.

As shown in Figure 4-2 the full system transient model started with the system at rest. The compressors then started at fixed speed and the system was allowed to come up to pressure. The compressor controllers then took over and drove to the initial target heat load of 650 kW and 400 kW in the top and bottom cycle condensers respectively by varying the compressor speeds, pictured in Figure 4-2. The valve controllers pictured in Figure 4-3 respond to changes in refrigerant superheat exiting the evaporator in each cycle precipitated by the change in compressor speed, attempting to maintain their 5 K superheat target. After steady operation was achieved, the target heat load was reduced to 550 kW in the top cycle condenser and 340kW in the bottom cycle

condenser. Once the system conditions had stabilized again, the requested steam load was changed back to 650 kW and allowed to stabilize once more.

Table 4-1: List of simulation events (Figures 4-2 to 4-5)

Event Number	Event name	Event Time
0	Simulation Start	0 s
1	Compressor start	3000 s
2	Compressor controller start	4500 s
3	EXV setpoint increase	7250 s
4	Turndown initiated	7500 s
5	EXV setpoint return	7750 s
6	Turnup initiated	10500 s
End	Simulation end	13500 s

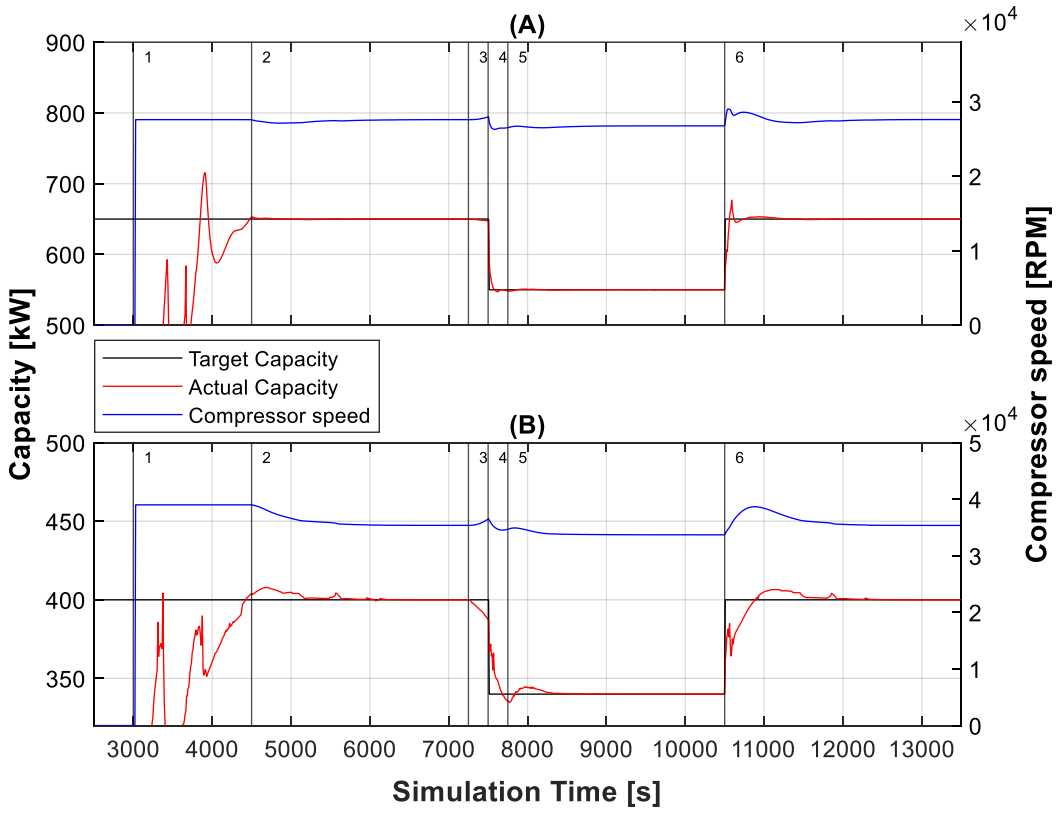

Figure 4-2: Compressor PID controller operation **(A)** – C-100/C-101 controller, **(B)** – C-200 controller

4.4 Expansion Valve Control

A turndown control strategy is needed particularly on the bottom cycle which does not have an SLHX to prevent liquid ingestion to the compressors. Liquid ingestion was prevented by increasing the superheat setpoint during the transition from full to part load just before liquid ingestion is likely to occur.

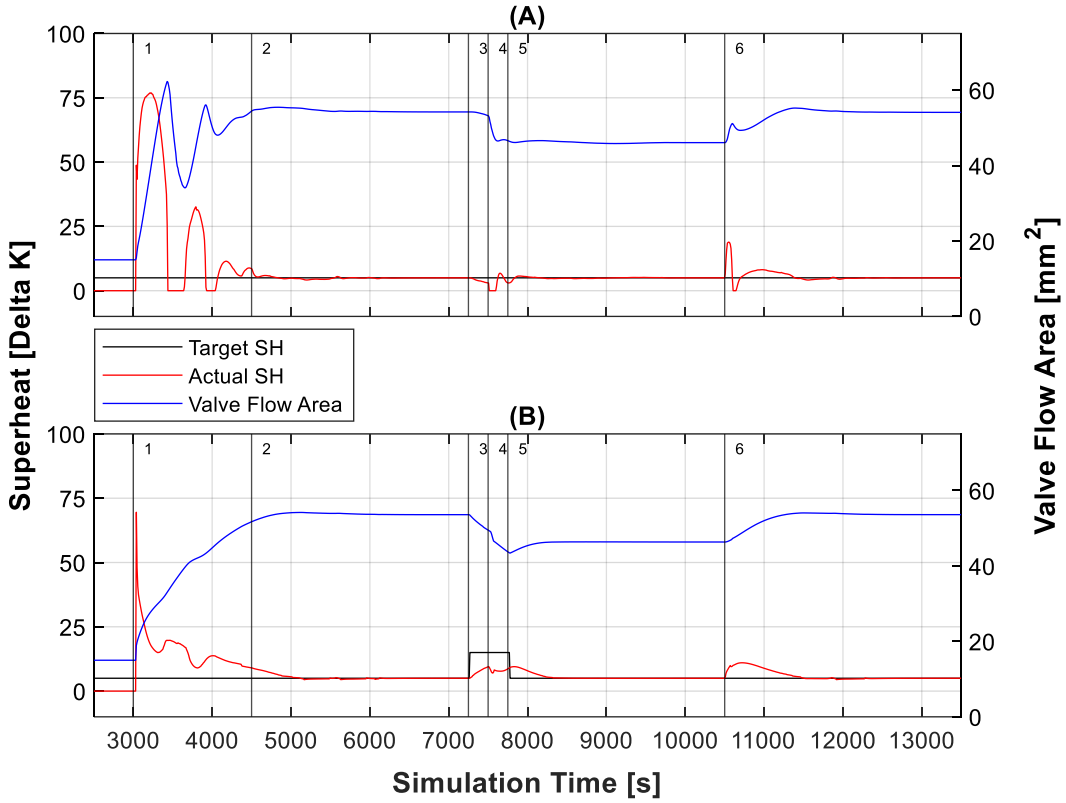

Figure 4-3: EXV controller operation for top and bottom cycles, **(A)** Top cycle EXV operation, **(B)** – Bottom cycle EXV operation

Beginning the system transition to turndown mode, the superheat target of the bottom cycle expansion valve was increased to 15 K before the compressor controller reduced its speed to meet the new setpoint. Once the new setpoint had been reached, the superheat target returned to 5 K. The elevated superheat target provided a buffer when a reduction in compressor speed resulted in both a reduced pressure ratio between the high and low sides of the cycle, and a reduced capacity

in the evaporator which had a compound effect of incomplete evaporation in the evaporator. This buffer allowed for a substantial transient drop in the superheat at the compressor's suction while still preventing liquid ingestion. This is not a concern for the top cycle as the refrigerant exiting the evaporator is passed through the SLHX which always superheats it well above the saturation temperature, as can be seen in Figure 4-4.

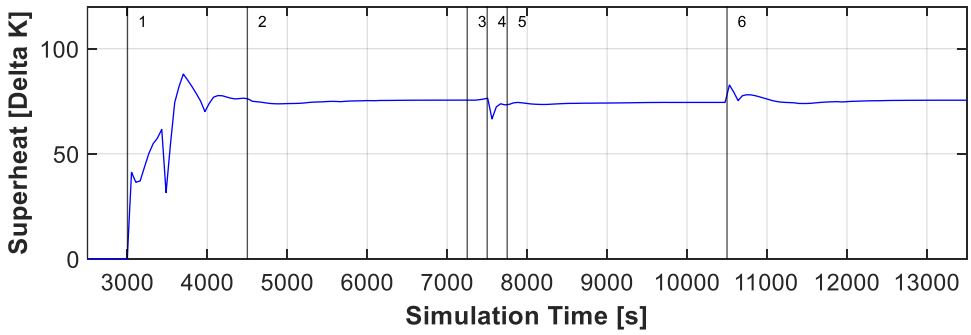

Figure 4-4: Refrigerant superheat at C-100 LP-1 suction

A comparison is made between the model with the liquid ingestion mitigation strategy (LIMS) and the one without in Figure 4-5. It can be seen that without the LIMS there is a liquid ingestion event during the transition to turndown, but with the LIMS implemented there is no such event.

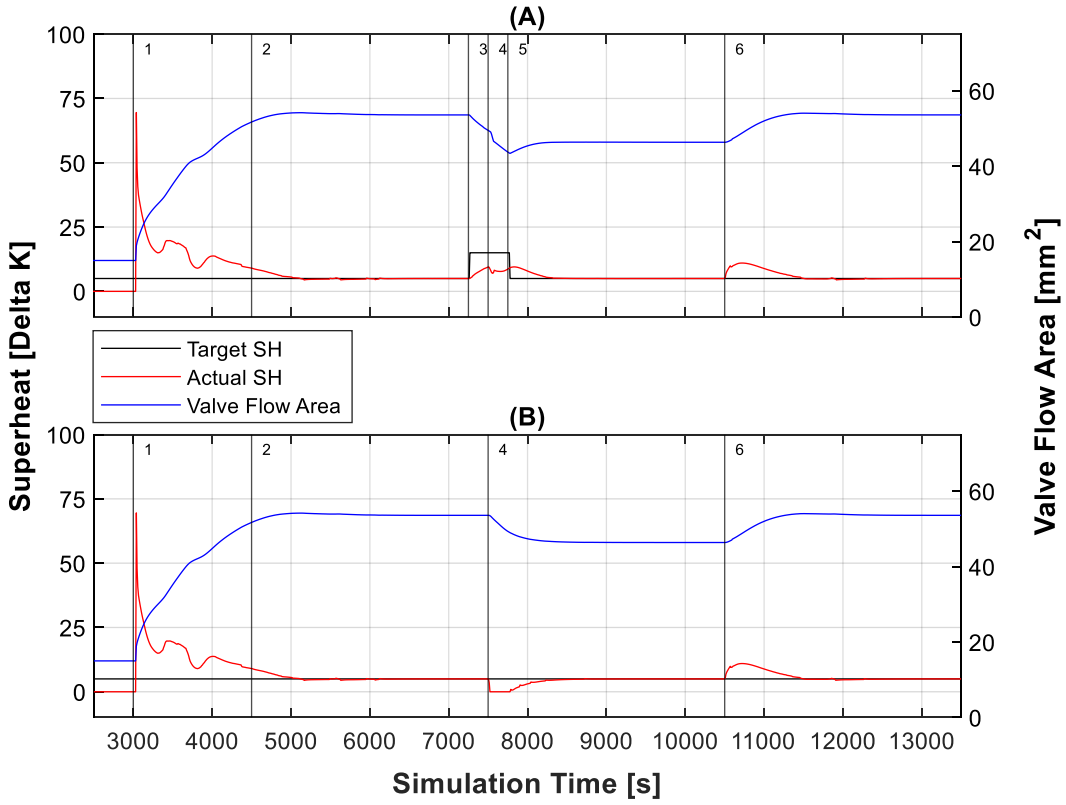

Figure 4-5: (A) - bottom cycle EXV performance with LIMS **(B)** - bottom cycle EXV performance without LIMS

4.5 Compressor Maps and Transients

Compressor operation was plotted on the compressor maps to confirm that the operating point always fell between the surge and choke lines during both full load, part load operation and transitional operation as shown in Figures 4-6, 4-7, and 4-8. It was found that the compressors operated within the bounds of the map during steady state operation at full load and part load, as well as during the transitions in-between. It was noted that the Bottom cycle compressor operated slightly outside the choke line both during both the most demanding transient operating points pictured in Figure 4-8 (C) and (D), and that for the deign point pictured in Figure 4-8 (A) it operated very close to, but inside the choke line. This operation is not necessarily ideal but does not pose the same risks to the compressor as operating in surge and is therefore acceptable.

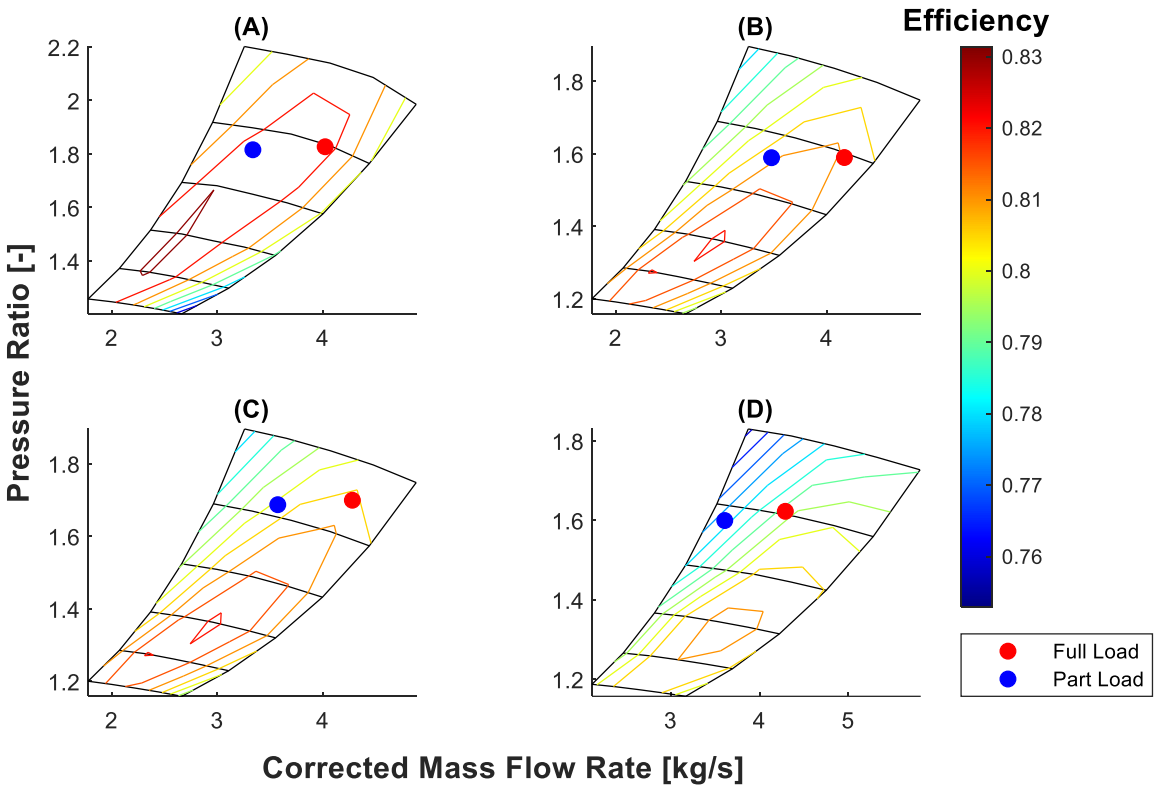

Figure 4-6: C-100 and C-101 compressor operating points during steady-state operation for full and part loads, **(A)** – LP-1 operation, **(B)** – LP-2 operation, **(C)** – HP-1 operation, **(D)** – HP-2 operation

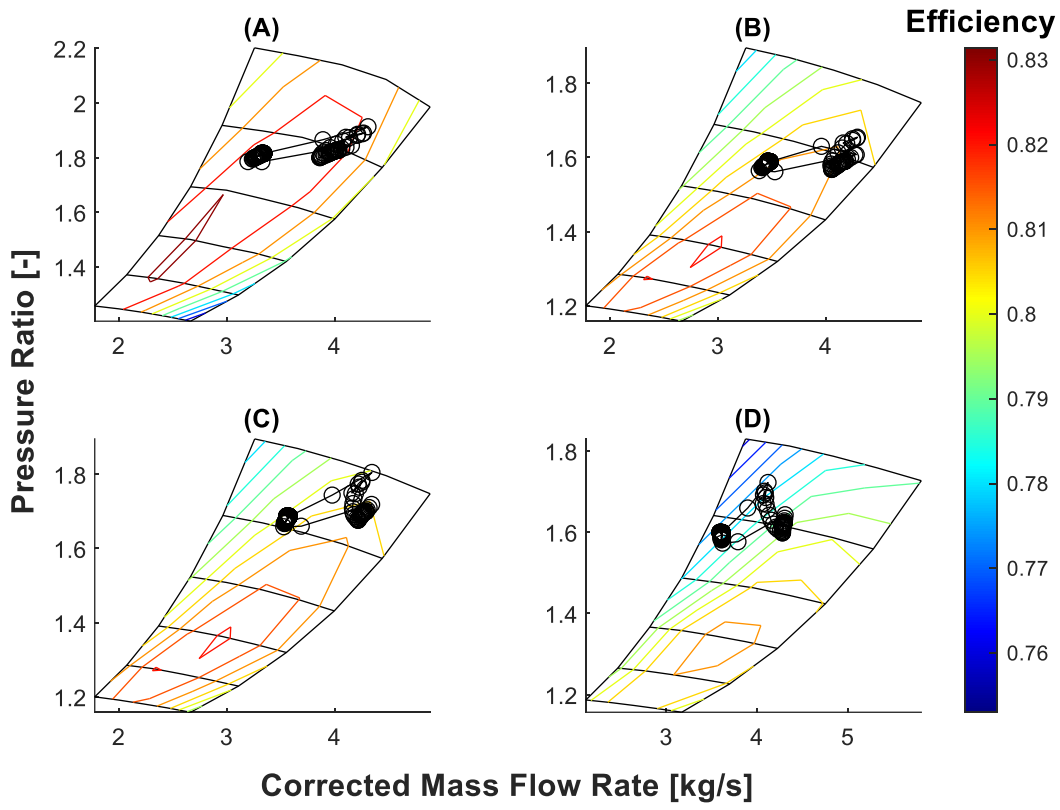

Figure 4-7: C-100 and C-101 compressor operation during load following from 7000s to 12500s, **(A)** – LP-1 operation, **(B)** – LP-2 operation, **(C)** – HP-1 operation, **(D)** – HP-2 operation

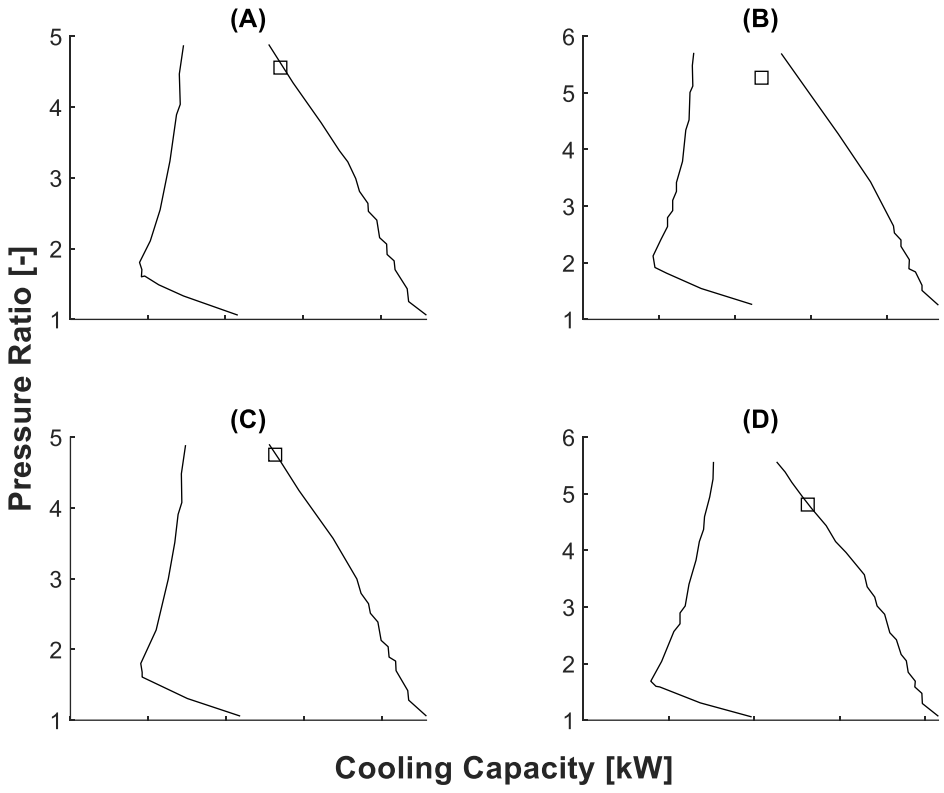

Figure 4-8: C-200 compressor operation at steady full load and part load operation as well as selected operating points during transients generated by inputting GT-SUITE operating data to the compressor Original Equipment Manufacturer (OEM) performance prediction tool. "Cooling Capacity" refers to the heat duty in the bottom cycle condenser as these machines are typically used in chillers, however the numerical values have been removed from this axis at the request of Danfoss. **(A)** – System Design point, **(B)** – Turndown operation, **(C), (D)** – selected transient operating points

4.5.1 COP Transients

The COPs of the individual cycles as well as the cumulative system COP were recorded for the duration of the simulation and are presented in Figure 4-9. Upon implementation of LIMS, there was a small increase in bottom cycle COP and a decrease in bottom cycle duty during the preparation to change, but adjustments in the top cycle controller made up for the loss of heat transfer in HX-140 so the net cycle effect was minimal both in terms of COP and steam supply capacity. Both the individual cycle and overall system COPs were seen to slightly increase during

turndown operation. This was due to several factors: Reduced pressure drops from lower refrigerant flow rates, closer temperature approaches in the heat exchangers, and constant glycol flow rate during turndown, which together resulted in both a higher glycol outlet temperature and a higher refrigerant outlet temperature from HX-240. This reduced the total temperature lift of the heat pump thereby increasing the COP of the individual and combined cycles during turndown.

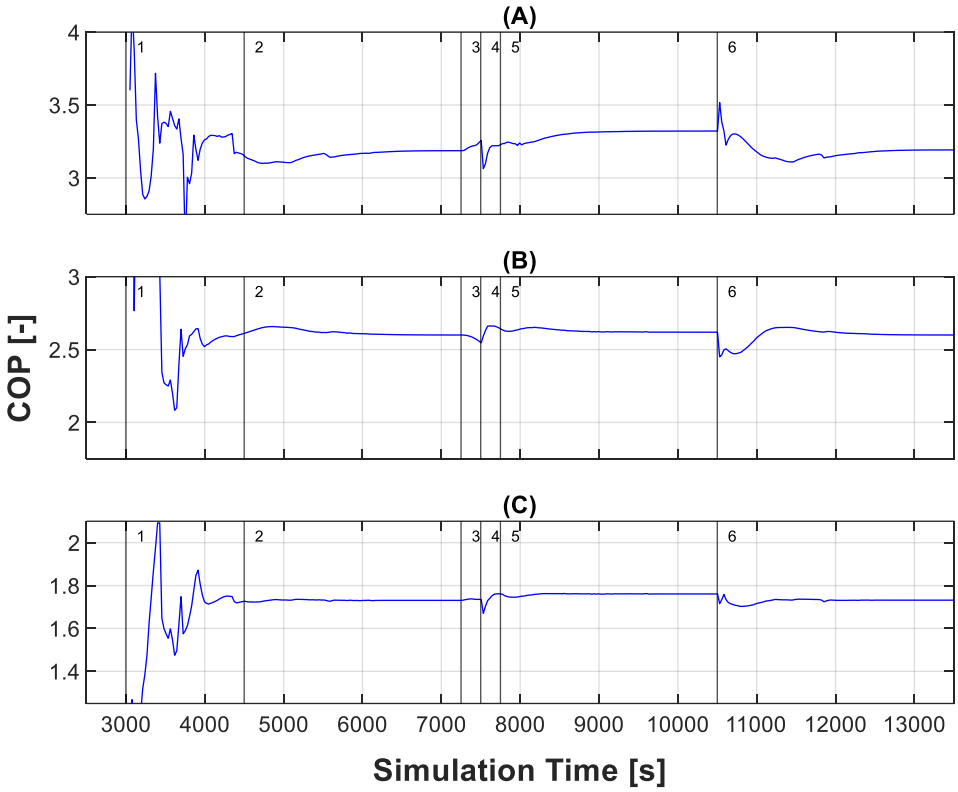

Figure 4-9: COP of individual and combined cycles, **(A)** – Bottom cycle COP, **(B)** – Top cycle COP, **(C)** – System overall COP

CHAPTER 5: Conclusion

A transient study of an ambient temperature source, centrifugal-compressor driven, steam-generating heat pump with steam delivery temperature of 150°C was conducted. An initial steady state model was used as a preliminary validation metric for an investigation of system transients during startup and load transitions. It was found that the result of the transient model under stable operation with optimized refrigerant charge agreed well with the desired operating state of the heat pump outlined by the initial steady state model. Transient conditions including cold startup to full load operation, full load operation to part load operation, and part load operation back to full load operation were modeled, and a strategy was developed for preventing liquid ingestion when transitioning to turndown operation. Compressor operation was evaluated during steady operation at full and part load and during load transitions. The compressors were found to operate at reasonable conditions during both steady and transitional operation. The system COP was predicted for both full and part load operation and in transition between them. It was found that the COP of both individual cycles as well as the overall system increased during turndown operation because of reduced pressure drops from lower refrigerant flow rates, closer temperature approaches in the heat exchangers, and constant glycol flow rate during turndown, which together result in both a higher glycol outlet temperature and a higher refrigerant outlet temperature from HX-240. The constant glycol flow rate results in a reduced total temperature lift of the heat pump thereby increasing the COP of the individual and combined cycles. Limitations to this work include bridging the gap between simulation controls-design and real-world implementation including but not restricted to factors like control valve actuation speed, control valve discharge coefficient variation with valve position, compressor motor and VFD power consumption considerations, and compressor rotor inertia. Future work could include: Model validation against test prototype once the prototype test facility is fully commissioned and test data is available, including data for

startup, steady operation, and load following; increased model fidelity through additions of electric motor models to drive the compressors; addition of air coil units air coils units; and implementation realistic outdoor temperature and humidity changes modeling frost accumulation on air coils and defrosting strategies. Future work could also include integration of additional performance enhancing system components and modeling of additional pilot heat pump configurations with realistic piping including bends and elevation changes and new heat exchanger designs. These model predictions can be used to improve the overall system design and streamline the commissioning process by eliminating the need for trial and error to determine required system charge.

REFERENCES

[1] V. Masson-Delmotte *et al.*, "Global warming of 1.5°C An IPCC Special Report on the impacts of global warming of 1.5°C above pre-industrial levels and related global greenhouse gas emission pathways, in the context of strengthening the global response to the threat of climate change, sustainable development, and efforts to eradicate poverty Edited by Science Officer Science Assistant Graphics Officer Working Group I Technical Support Unit," 2019. Accessed: Jun. 23, 2024. [Online]. Available: https://www.ipcc.ch/sr15/download/

[2] G. P. Thiel and A. K. Stark, "To decarbonize industry, we must decarbonize heat," *Joule*, vol. 5, no. 3, pp. 531–550, Mar. 2021, doi: 10.1016/j.joule.2020.12.007.

[3] J. Rissman, "Decarbonizing Low-Temperature Industrial Heat in the." Accessed: Jun. 22, 2024. [Online]. Available: https://energyinnovation.org/wp-content/uploads/2022/10/Decarbonizing-Low-Temperature-Industrial-Heat-In-The-U.S.-Report-2.pdf

[4] US EPA, "Power Sector Evolution." Accessed: Feb. 03, 2024. [Online]. Available: https://www.epa.gov/power-sector/power-sector-evolution

[5] The Renewable Thermal Collaborative, "RTC Vision Report," The Renewable Thermal Collaborative . Accessed: May 20, 2024. [Online]. Available: https://www.renewablethermal.org/wp-content/uploads/2018/06/RTC-Vision-Report-Exec-Summary-FINAL-1.pdf

[6] Y. A. Çengel, M. A. Boles, and M. Kanoğlu, *Thermodynamics: An Engineering Approach, Ninth Edition*, 9th ed. 2019.

[7] C. Arpagaus, F. Bless, M. Uhlmann, J. Schiffmann, and S. S. Bertsch, "High temperature heat pumps: Market overview, state of the art, research status, refrigerants, and application potentials," *Energy*, vol. 152, pp. 985–1010, Jun. 2018, doi: 10.1016/j.energy.2018.03.166.

[8] B. Zühlsdorf, "IEA Annex 58 Task 1: Technologies – State of the art and ongoing developments for systems and components." Accessed: Jan. 22, 2024. [Online]. Available: https://heatpumpingtechnologies.org/annex58/task1/

[9] T. Wright and P. M. Gerhart, *Fluid machinery : application, selection, and design*. CRC Press, 2010.

[10] Seán Moran, "How to design a process control system," *An Applied Guide to Process and Plant Design*, 2015.

[11] O. E. Balje, "A Study on Design Criteria and Matching of Turbomachines: Part B Compressor and Pump Performance and Matching of Turbocomponents." [Online].

Available: http://asmedigitalcollection.asme.org/gasturbinespower/article-pdf/84/1/103/5804523/103_1.pdf

[12] K. E. Nichols, "How to Select Turbomachinery For Your Application." Accessed: Jun. 23, 2024. [Online]. Available: https://barber-nichols.com/wp-content/uploads/2019/11/how_to_select_turbomachinery_for_your_application.pdf

[13] A. Gużda and N. Szmolke, "Compressors in Heat Pumps," *Machine Dynamics Research*, vol. 39, no. 2, pp. 71–83, 2015, [Online]. Available: https://www.researchgate.net/publication/313134829

[14] D. Snow, *Plant Engineer's Reference Book, Second Edition*. 2002.

[15] A. Beyene and P. Lowrey, "Strategies to raise the off-design efficiency of chiller machines," *Int J Energy Res*, vol. 20, no. 7, pp. 625–636, 1996, doi: 10.1002/(SICI)1099-114X(199607)20:7<625::AID-ER177>3.0.CO;2-J.

[16] F. Bless, C. Arpagaus, S. S. Bertsch, and J. Schiffmann, "Theoretical analysis of steam generation methods - Energy, CO2 emission, and cost analysis," *Energy*, vol. 129, pp. 114–121, 2017, doi: 10.1016/j.energy.2017.04.088.

[17] S. Briola, S. Barberis, M. Renzi, and R. Gabbrielli, "Theoretical investigation of a novel high-temperature heat pump exploiting low-temperature waste heat and using two-phase machines with zero electric consumption," *Appl Therm Eng*, vol. 235, Nov. 2023, doi: 10.1016/j.applthermaleng.2023.121322.

[18] X. Q. Cao, W. W. Yang, F. Zhou, and Y. L. He, "Performance analysis of different high-temperature heat pump systems for low-grade waste heat recovery," *Appl Therm Eng*, vol. 71, no. 1, pp. 291–300, Oct. 2014, doi: 10.1016/j.applthermaleng.2014.06.049.

[19] S. Cui, S. Geng, J. Bai, Y. Zhang, S. Guan, and H. Yang, "High Temperature Cascade Heat Pump System With Double Medium and Low Temperature Heat Sources," *Thermal Science*, vol. 27, no. 3, pp. 1835–1843, 2023, doi: 10.2298/TSCI2303835C.

[20] X. Li *et al.*, "Performance analysis of high-temperature water source cascade heat pump using BY3B/BY6 as refrigerants," *Appl Therm Eng*, vol. 159, Aug. 2019, doi: 10.1016/j.applthermaleng.2019.113895.

[21] J. Wu, Z. Yang, Q. Wu, and Y. Zhu, "Transient behavior and dynamic performance of cascade heat pump water heater with thermal storage system," *Appl Energy*, vol. 91, no. 1, pp. 187–196, 2012, doi: 10.1016/J.APENERGY.2011.09.020.

[22] H. Yan, B. Hu, and R. Wang, "Air-source heat pump heating based water vapor compression for localized steam sterilization applications during the COVID-19 pandemic," *Renewable and Sustainable Energy Reviews*, vol. 145, Jul. 2021, doi: 10.1016/j.rser.2021.111026.

[23] C. K. Lee, "Dynamic performance of ground-source heat pumps fitted with frequency inverters for part-load control," *Appl Energy*, vol. 87, no. 11, pp. 3507–3513, 2010, doi: 10.1016/j.apenergy.2010.04.029.

[24] S. Malavika *et al.*, "Performance optimization of a heat pump for high temperature application," in *Materials Today: Proceedings*, Elsevier Ltd, 2020, pp. 5278–5285. doi: 10.1016/j.matpr.2020.08.639.

[25] L. Xu, M. Li, Y. Zhang, and X. Luo, "Applicability and comparison of solar-air source heat pump systems between cold and warm regions of plateau by transient simulation and experiment," *Build Simul*, vol. v 14, n 6, no. 6, p. p 1697-1708, Dec. 2021, doi: 10.1007/s12273-020-0748-5.

[26] S. M. Hosseinnia, L. Amiri, H. Nesreddine, D. Monney, and S. Poncet, "Thermodynamic analysis of high temperature cascade heat pump with R718 (high stage) and six different low-GWP refrigerants (low stage)," *Case Studies in Thermal Engineering*, vol. 53, Jan. 2024, doi: 10.1016/j.csite.2023.103812.

[27] U. Tomc *et al.*, "Small demonstrator of a thermoelectric heat-pump booster for an ultra-low-temperature district-heating substation," *Appl Energy*, vol. 361, May 2024, doi: 10.1016/j.apenergy.2024.122899.

[28] A. J. Pimm, T. T. Cockerill, and W. F. Gale, "Reducing industrial hydrogen demand through preheating with very high temperature heat pumps," *Appl Energy*, vol. 347, Oct. 2023, doi: 10.1016/j.apenergy.2023.121464.

[29] J. V. M. Walden, B. Wellig, and P. Stathopoulos, "Heat pump integration in non-continuous industrial processes by Dynamic Pinch Analysis Targeting," *Appl Energy*, vol. 352, Dec. 2023, doi: 10.1016/j.apenergy.2023.121933.

[30] T. Kaida, I. Sakuraba, K. Hashimoto, and H. Hasegawa, "Experimental performance evaluation of heat pump-based steam supply system," in *IOP Conference Series: Materials Science and Engineering*, Institute of Physics Publishing, Jul. 2015. doi: 10.1088/1757-899X/90/1/012076.

[31] D. H. Kang, S. I. Na, J. W. Yoo, J. H. Lee, and M. S. Kim, "Experimental study on the performance of a steam generation heat pump with the internal heat exchanging effect," *International Journal of Refrigeration*, vol. 108, pp. 154–162, Dec. 2019, doi: 10.1016/j.ijrefrig.2019.09.003.

[32] S. Koundinya, J. Jothilingam, and S. Seshadri, "Low-pressure steam generating heat pump – A design and field implementation case study," *Thermal Science and Engineering Progress*, p. 102140, Sep. 2023, doi: 10.1016/j.tsep.2023.102140.

[33] T. Oue and K. Okada, "Air-sourced 90°C Hot Water Supplying Heat Pump 'HEM-90A,'" 2013. Accessed: Jun. 23, 2024. [Online]. Available: https://www.kobelco.co.jp/english/ktr/pdf/ktr_32/070-074.pdf

[34] S. T. Kim, R. Hegner, G. Özuylasi, P. Stathopoulos, and E. Nicke, "Performance analysis of multistage high-temperature heat pump cycle," *Energy Sci Eng*, 2023, doi: 10.1002/ese3.1536.

[35] J. S. Lee, H. Park, and Y. Kim, "Transient performance characteristics of a hybrid ground-source heat pump in the cooling mode," *Appl Energy*, vol. 123, pp. 121–128, Jun. 2014, doi: 10.1016/j.apenergy.2014.02.056.

[36] N. Deng, M. Zhou, Z. Zhang, Y. Zhang, H. Wang, and X. Li, "Experimental Research of a New Steam Heat Pump System for Recovering Industrial Waste Heat", doi: 10.1061/(ASCE)EY.1943-7897.0000458.

[37] K. Wang, F. Cao, and Z. Xing, "Development and experimental validation of a high-temperature heat pump for heat recovery and building heating," *Energy Build*, vol. 41, no. 7, pp. 732–737, Jul. 2009, doi: 10.1016/j.enbuild.2009.02.004.

[38] S. Boahen *et al.*, "Capacity control of a cascade multi-purpose heat pump using variable speed compressor," *Renew Energy*, vol. 205, pp. 945–955, Mar. 2023, doi: 10.1016/j.renene.2023.02.002.

[39] J. Gao, S. Li, F. Wu, L. Jiang, Y. Zhao, and X. Zhang, "Study on efficient heating method by solar coupled air source heat pump system with phase change heat storage in severe cold region," *Appl Energy*, vol. 367, Aug. 2024, doi: 10.1016/j.apenergy.2024.123206.

[40] X. Guo, J. Zhang, and Y. Han, "Thermoelectric performance analysis of the novel direct-expansion photovoltaic thermal heat pump/power heat pipe compound cycle system in summer," *Appl Energy*, vol. 362, May 2024, doi: 10.1016/j.apenergy.2024.122969.

[41] M. Chamoun, R. Rulliere, P. Haberschill, and J. F. Berail, "Dynamic model of an industrial heat pump using water as refrigerant," *International Journal of Refrigeration*, vol. 35, no. 4, pp. 1080–1091, Jun. 2012, doi: 10.1016/J.IJREFRIG.2011.12.007.

[42] D. Ndiaye and M. Bernier, "Transient model of a geothermal heat pump in cycling conditions - Part A: The model," *International Journal of Refrigeration*, vol. 35, no. 8, pp. 2110–2123, Dec. 2012, doi: 10.1016/J.IJREFRIG.2012.08.013.

[43] D. Ndiaye and M. Bernier, "Transient model of a geothermal heat pump in cycling conditions - Part B: Experimental validation and results," *International Journal of Refrigeration*, vol. 35, no. 8, pp. 2124–2137, Dec. 2012, doi: 10.1016/J.IJREFRIG.2012.08.015.

[44] P. Nenkaew and C. Tangthieng, "Effect of transient heat transfer of a condenser on a cascade heat pump performance," *Engineering Journal*, vol. 20, no. 3, pp. 49–61, Aug. 2016, doi: 10.4186/EJ.2016.20.3.49.

[45] E. Bellos *et al.*, "Investigation of a High-Temperature Heat Pump for Heating Purposes," *Applied Sciences (Switzerland)*, vol. 13, no. 4, Feb. 2023, doi: 10.3390/app13042072.

[46] J. Park *et al.*, "Assessment of energy self-sufficiency of a smart farm through integrated modeling of air-source heat pumps and solar power generation," *Appl Energy*, vol. 367, Aug. 2024, doi: 10.1016/j.apenergy.2024.123398.

[47] Y. Wang, Z. Quan, Y. Zhao, L. Wang, and Z. Liu, "Performance and optimization of a novel solar-air source heat pump building energy supply system with energy storage," *Appl Energy*, vol. 324, Oct. 2022, doi: 10.1016/j.apenergy.2022.119706.

[48] M. Chamoun, R. Rulliere, P. Haberschill, and J. L. Peureux, "Modelica-based modeling and simulation of a twin screw compressor for heat pump applications," *Appl Therm Eng*, vol. 58, no. 1–2, pp. 479–489, 2013, doi: 10.1016/j.applthermaleng.2013.04.020.

[49] M. Zamojski, P. Sumerauer, C. Bacher, and F. Dohnal, "Towards Online Transient Simulation of a Real Heat Pump," *Springer Proceedings in Mathematics and Statistics*, vol. v 362, p. p 69-78, 2022, doi: 10.1007/978-3-030-77306-9_7.

[50] R. Huang, A. Mahvi, N. James, E. Kozubal, and J. Woods, "Evaluation of phase change thermal storage in a cascade heat pump," *Appl Energy*, vol. 359, Apr. 2024, doi: 10.1016/j.apenergy.2024.122654.

[51] J. J. Aguilera, W. Meesenburg, W. B. Markussen, B. Zühlsdorf, and B. Elmegaard, "Real-time monitoring and optimization of a large-scale heat pump prone to fouling - towards a digital twin framework," *Appl Energy*, vol. 365, p. 123274, Jul. 2024, doi: 10.1016/j.apenergy.2024.123274.

[52] H. Okazaki, H. Ono, and N. Yanai, "Optimization of start-up operation for centrifugal chiller," in *IFAC-PapersOnLine*, Elsevier B.V., Jul. 2022, pp. 332–337. doi: 10.1016/j.ifacol.2022.09.046.

[53] P. Schalbart and P. Haberschill, "Simulation of the behaviour of a centrifugal chiller during quick start-up," *International Journal of Refrigeration*, vol. 36, no. 1, pp. 222–236, Jan. 2013, doi: 10.1016/j.ijrefrig.2012.09.015.

[54] P. Li, Y. Li, and J. E. Seem, "Dynamic Modeling and Stability Analysis of Water-Cooled Centrifugal Chillers," 2010. [Online]. Available: http://asmedigitalcollection.asme.org/DSCC/proceedings-pdf/DSCC2010/44182/703/2704545/703_1.pdf

[55] M. W. Browne and P. K. Bansal, "Transient simulation of vapour-compression packaged liquid chillers." doi: 10.1016/S0140-7007(01)00060-3.

[56] W. J. Zhang, C. L. Zhang, and G. L. Ding, "Transient modeling of an air-cooled chiller with economized compressor. Part I: Model development and validation," *Appl Therm Eng*, vol. 29, no. 11–12, pp. 2396–2402, Aug. 2009, doi: 10.1016/j.applthermaleng.2008.12.012.

[57] W. J. Zhang, S. F. Ding, and C. L. Zhang, "Transient modeling of an air-cooled chiller with economized compressor. Part II: Application to control design," *Appl Therm Eng*,

vol. 29, no. 11–12, pp. 2403–2407, Aug. 2009, doi: 10.1016/j.applthermaleng.2008.12.007.

[58] M. Zhao, G. Shu, H. Tian, F. Yan, G. Huang, and C. Hu, "The investigation of the Recuperative Organic Rankine Cycle models for the waste heat recovery on vehicles," in *Energy Procedia*, Elsevier Ltd, 2017, pp. 732–739. doi: 10.1016/j.egypro.2017.09.106.

[59] X. Li *et al.*, "Preliminary tests on dynamic characteristics of a CO2 transcritical power cycle using an expansion valve in engine waste heat recovery," *Energy*, vol. 140, pp. 696–707, 2017, doi: 10.1016/j.energy.2017.09.022.

[60] X. Li *et al.*, "Experimental comparison of dynamic responses of CO2 transcritical power cycle systems used for engine waste heat recovery," *Energy Convers Manag*, vol. 161, pp. 254–265, Apr. 2018, doi: 10.1016/j.enconman.2018.02.010.

[61] X. Li, H. Tian, G. Shu, C. Hu, R. Sun, and L. Li, "Effects of external perturbations on dynamic performance of carbon dioxide transcritical power cycles for truck engine waste heat recovery," *Energy*, vol. 163, pp. 920–931, Nov. 2018, doi: 10.1016/j.energy.2018.08.137.

[62] X. Li, H. Tian, G. Shu, M. Zhao, C. N. Markides, and C. Hu, "Potential of carbon dioxide transcritical power cycle waste-heat recovery systems for heavy-duty truck engines," *Appl Energy*, vol. 250, pp. 1581–1599, Sep. 2019, doi: 10.1016/j.apenergy.2019.05.082.

[63] N.-H. and H. A. and R. G. and A. R. Lehocky Marek and Framke, "Application of 1D Numerical Transient Compressor Model to Optimize Performance of Vapor Injection Heat Pump System," in *13th International Conference on Compressors and Their Systems*, S. and I.-K. I. and K. A. Read Matthew and Rane, Ed., Cham: Springer Nature Switzerland, 2024, pp. 339–353. doi: 10.1007/978-3-031-42663-6_28.

[64] O. Kaplan, "Heat Pump System Modeling," in *GT Conference 2012*, 2012. Accessed: Jun. 16, 2024. [Online]. Available: https://www.gtisoft.com/wp-content/uploads/publication/HeatPumpSystemModelingIAV.pdf

[65] M. Bhaskar and S. Design Engineer, "Heat Pump Water Heater Design in GT-SUITE," in *GT Conference 2019* , 2019. Accessed: Jun. 16, 2024. [Online]. Available: https://www.gtisoft.com/wp-content/uploads/2020/03/Rheem_GT_USConference_2019.pdf

[66] M. Wilson, "Heat Pump Systems with Heat Exchange to Liquid and Air ," in *GT Conference 2019*, Nov. 2019. Accessed: Jun. 23, 2024. [Online]. Available: https://www.gtisoft.com/wp-content/uploads/2019/12/Heat-Pump-Systems-with-Heat-Exchange-to-Liquid-and-Air-Michael-Wilson-Daikin.pdf

APPENDIX A. Heat exchanger calibration data

Table A-1: HX-110 performance calibration data

Mass flow rate [kg/s]	Main inlet temperature [C]	Main inlet pressure [kPa]	Main outlet pressure [kPa]	Secondary mass flow rate [kg/s]	Secondary inlet temperature [C]	Secondary inlet pressure [kPa]	Secondary outlet pressure [kPa]	Heat transfer rate [kW]
3.78	204.78	2985.43	2956.85	0.26	148.0	481.84	478.89	560.3
4.03	204.78	2985.43	2953.11	0.28	148.0	481.84	478.45	597.95
4.28	204.78	2985.43	2949.07	0.3	148.0	481.84	478.05	635.43
4.41	204.78	2985.43	2947.08	0.31	148.0	481.84	477.86	653.91
4.54	204.78	2985.43	2944.87	0.32	148.0	481.84	477.66	673.7
4.79	204.78	2985.43	2940.68	0.33	148.0	481.84	477.27	710.04
5.04	204.78	2985.43	2936.03	0.35	148.0	481.84	476.92	747.5
5.29	204.78	2985.43	2931.18	0.37	148.0	481.84	476.54	784.82
5.54	204.78	2985.43	2925.8	0.39	148.0	481.84	476.13	822.29

	Attribute	Unit	Object Value
Heat Exchanger Model Setup			
	Component Fluids (Main:Secondary)		Refrigerant:Refrigerant
	Heat Exchanger Model		Empirical Correlations
	Heat Exchanger Discretization		Number of Subvolumes
	Number of Subvolumes		50
Overall Geometry			
	Heat Exchanger Construction		
	Shell and Tube		
◉	Number of Tubes (Nt)		580
◉	Inlet Tank Volume	L	17.4
◉	Outlet Tank Volume	L	17.4
○	Concentric Tube		
	Tube Length (L)	ft	6
Main Connection Geometry			
	Inlet Connection Diameter (Dm1)	in	6
☐	Inlet Orifice Diameter	mm	
	Outlet Connection Diameter (Dm2)	in	3
☐	Outlet Orifice Diameter	mm	
Heat Exchanger Mass			
◉	Automatically Calculate Dry Mass		
○	Total Core Dry Mass	kg	

Figure A-1: HX-110 geometry input

Table A-2: HX-140 performance calibration data

Mass flow rate [kg/s]	Main inlet vapor quality [-]	Main inlet pressure [kPa]	Main outlet pressure [kPa]	Secondary mass flow rate [kg/s]	Secondary inlet temperature [C]	Secondary inlet pressure [kPa]	Secondary outlet pressure [kPa]	Heat transfer rate [kW]
2.782	0.34	418.8	412.74	2.38	81.21	1972.63	1972.04	328.28
3.273	0.34	420.6	412.47	2.79	81.21	1972.73	1971.93	383.02
3.596	0.34	421.7	412.07	3.06	81.21	1972.79	1971.84	415.53
3.764	0.34	422.4	411.97	3.2	81.21	1972.83	1971.79	429.21
4.255	0.34	424.2	411.34	3.61	81.21	1972.92	1971.58	458.87
4.745	0.34	426.0	410.55	4.02	81.21	1973.01	1971.31	481.63
5.727	0.34	429.8	408.6	4.84	81.21	1973.21	1970.63	517.52

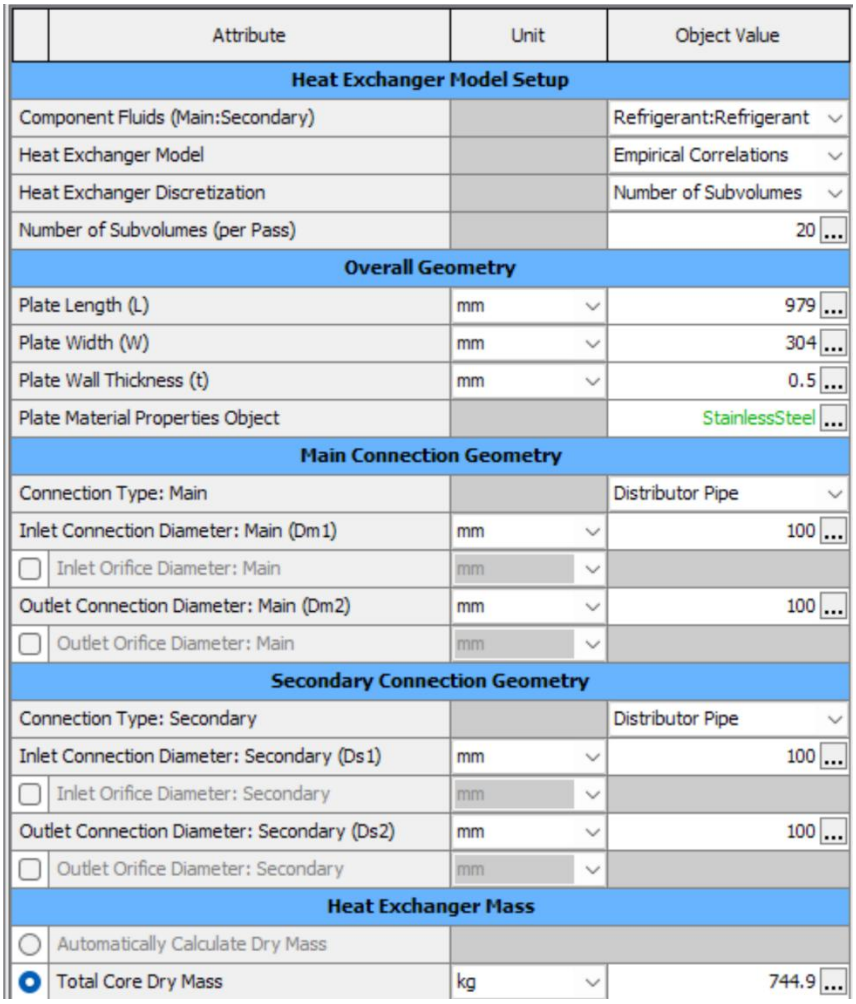

Figure A-2: HX-140 geometry input

Table A-3: HX-130-SLHX performance calibration data

Mass flow rate [kg/s]	Main inlet temperature [C]	Main inlet pressure [kPa]	Main outlet pressure [kPa]	Secondary mass flow rate [kg/s]	Secondary inlet temperature [C]	Secondary inlet pressure [kPa]	Secondary outlet pressure [kPa]	Heat transfer rate [kW]
7.14	146.9	2889.26	2887.0	7.368	67.59	411.3	383.3	420.8
6.6045	146.9	2888.94	2887.0	6.8154	67.59	407.3	383.3	389.2
6.069	146.9	2888.65	2887.0	6.2628	67.59	403.6	383.3	357.6
5.5335	146.9	2888.38	2887.0	5.7102	67.59	400.2	383.3	326.2
4.998	146.9	2888.13	2887.0	5.1576	67.59	397.1	383.3	294.6
4.4625	146.9	2887.907	2887.0	4.605	67.59	394.3	383.3	263.0
3.927	146.9	2887.708	2887.0	4.0524	67.59	391.87	383.3	231.4
3.57	146.9	2887.589	2887.0	3.684	67.59	390.4	383.3	210.4
3.3915	146.9	2887.533	2887.0	3.4998	67.59	389.72	383.3	199.84
2.856	146.9	2887.384	2887.0	2.9472	67.59	387.87	383.3	168.28
2.3205	146.9	2887.259	2887.0	2.3946	67.59	386.34	383.3	136.7
1.785	146.9	2887.158	2887.0	1.842	67.59	385.11	383.3	105.16

Attribute	Unit	Object Value
Heat Exchanger Model Setup		
Component Fluids (Main:Secondary)		Refrigerant:Refrigerant
Heat Exchanger Model		Empirical Correlations
Heat Exchanger Discretization		Number of Subvolumes
Number of Subvolumes (per Pass)		20
Overall Geometry		
Plate Length (L)	mm	374
Plate Width (W)	mm	364
Plate Wall Thickness (t)	mm	0.5
Plate Material Properties Object		StainlessSteel
Main Connection Geometry		
Connection Type: Main		Distributor Pipe
Inlet Connection Diameter: Main (Dm1)	mm	80
☐ Inlet Orifice Diameter: Main	mm	
Outlet Connection Diameter: Main (Dm2)	mm	80
☐ Outlet Orifice Diameter: Main	mm	
Secondary Connection Geometry		
Connection Type: Secondary		Distributor Pipe
Inlet Connection Diameter: Secondary (Ds1)	mm	100
☐ Inlet Orifice Diameter: Secondary	mm	
Outlet Connection Diameter: Secondary (Ds2)	mm	100
☐ Outlet Orifice Diameter: Secondary	mm	
Heat Exchanger Mass		
○ Automatically Calculate Dry Mass		
◉ Total Core Dry Mass	kg	118

Figure A-3: HX-130-SLHX geometry input

Table A-4: HX-240 performance calibration data

Mass flow rate [kg/s]	Main inlet vapor quality [-]	Main inlet pressure [kPa]	Main outlet pressure [kPa]	Secondary mass flow rate [kg/s]	Secondary inlet temperature [C]	Secondary inlet pressure [kPa]	Secondary outlet pressure [kPa]	Heat transfer rate [kW]
1.394	0.30421859	430.16	428.55	8.71	15.0	403.79	400.36	171.32
1.642	0.306624413	427.94	425.77	10.25	15.0	404.88	400.32	201.41
1.89	0.308769196	425.78	422.96	11.79	15.0	406.08	400.25	231.78
2.278	0.313031495	421.2	417.18	14.18	15.0	408.19	400.1	280.73
2.472	0.314212888	419.98	415.3	15.38	15.0	409.53	400.18	304.55
2.722	0.316139013	418.0	412.38	16.91	15.0	411.4	400.33	335.44
2.974	0.318375707	416.1	409.44	18.45	15.0	413.4	400.46	366.23
3.226	0.320385486	414.3	406.52	19.99	15.0	415.5	400.56	397.03
3.478	0.322736412	412.2	403.19	21.52	15.0	417.8	400.74	427.7
3.732	0.325410813	409.5	399.14	23.06	15.0	420.3	400.97	458.94
3.986	0.327268511	407.9	396.13	24.6	15.0	422.9	401.18	489.7
4.156	0.328767508	406.8	394.03	25.62	15.0	424.7	401.33	510.12

Attribute	Unit	Object Value
Heat Exchanger Model Setup		
Component Fluids (Main:Secondary)		Refrigerant:Liquid
Heat Exchanger Model		Empirical Correlations
Heat Exchanger Discretization		Number of Subvolumes
Number of Subvolumes (per Pass)		20
Overall Geometry		
Plate Length (L)	mm	694
Plate Width (W)	mm	304
Plate Wall Thickness (t)	mm	0.5
Plate Material Properties Object		StainlessSteel
Main Connection Geometry		
Connection Type: Main		Distributor Pipe
Inlet Connection Diameter: Main (Dm1)	mm	100
☐ Inlet Orifice Diameter: Main	mm	
Outlet Connection Diameter: Main (Dm2)	mm	100
☐ Outlet Orifice Diameter: Main	mm	
Secondary Connection Geometry		
Connection Type: Secondary		Distributor Pipe
Inlet Connection Diameter: Secondary (Ds1)	mm	73
☐ Inlet Orifice Diameter: Secondary	mm	
Outlet Connection Diameter: Secondary (Ds2)	mm	73
☐ Outlet Orifice Diameter: Secondary	mm	
Heat Exchanger Mass		
○ Automatically Calculate Dry Mass		
◉ Total Core Dry Mass	kg	310.86

Figure A-4: HX-240 geometry input